SpurLens: Automatic Detection of Spurious Cues in Multimodal LLMs

Anonymous authors
Paper under double-blind review

Abstract

Unimodal vision models are known to rely on spurious correlations, but it remains unclear to what extent Multimodal Large Language Models (MLLMs) exhibit similar biases despite language supervision. In this paper, we investigate spurious bias in MLLMs and introduce SpurLens, a pipeline that leverages GPT-4 and open-set object detectors to automatically identify spurious visual cues without human supervision. Our findings reveal that spurious correlations cause two major failure modes in MLLMs: (1) over-reliance on spurious cues for object recognition, where removing these cues reduces accuracy, and (2) object hallucination, where spurious cues amplify the hallucination by over 10x. We investigate various MLLMs and datasets, and validate our findings with multiple robustness checks. Beyond diagnosing these failures, we explore potential mitigation strategies, such as prompt ensembling and reasoning-based prompting, and conduct ablation studies to examine the root causes of spurious bias in MLLMs. By exposing the persistence of spurious correlations, our study calls for more rigorous evaluation methods and mitigation strategies to enhance the reliability of MLLMs.

1 Introduction

Multimodal large language models (MLLMs) (Wang et al., 2024; Liu et al., 2024a; Meta, 2024; OpenAI, 2024a) have seen rapid advances in recent years. These models leverage the powerful capabilities of large language models (LLMs) (OpenAI, 2024b; Touvron et al., 2023) to process diverse modalities, such as images and text. They have demonstrated significant proficiency in tasks such as image perception, visual question answering, and instruction following.

Despite these advancements, MLLMs still exhibit critical visual shortcomings (Tong et al., 2024a;b). One such failure is object hallucination (Li et al., 2023; Hu et al., 2023; Lovenia et al., 2023; Leng et al., 2024), where MLLMs generate semantically coherent but factually incorrect content, falsely detecting objects that are not present in the input images, as exemplified in Figure 1. We hypothesize that many of these failures stem from a well-known robustness issue in deep learning models: spurious bias – the tendency to rely on non-essential input attributes rather than truly recognizing the target object (Ye et al., 2024). While spurious correlation reliance has been well-documented in single-modality image classifiers, the extent to which it persists in MLLMs remains unclear.

Understanding spurious correlations is crucial because they can lead to systematic failures. Consider the case of a fire hydrant (Figure 2). When a fire hydrant appears in a street scene, Llama-3.2 (Meta, 2024) correctly recognizes it 96% of the time. However, when placed in unusual contexts, such as a warehouse, accuracy drops to 83%, suggesting an over-reliance on contextual cues rather than the object itself. Conversely, when shown a street scene without a fire hydrant, the model hallucinates its presence 7 times more often than when given a random image without a hydrant, such as an indoor environment lacking street-like features.

In this work, we systematically study spurious bias in MLLMs. We introduce *SpurLens*, a pipeline designed to rank images based on the presence of spurious cues. For each object, we leverage GPT-4 to generate a list of potential spurious cues and then rank images using open-set object detectors that assess the presence of

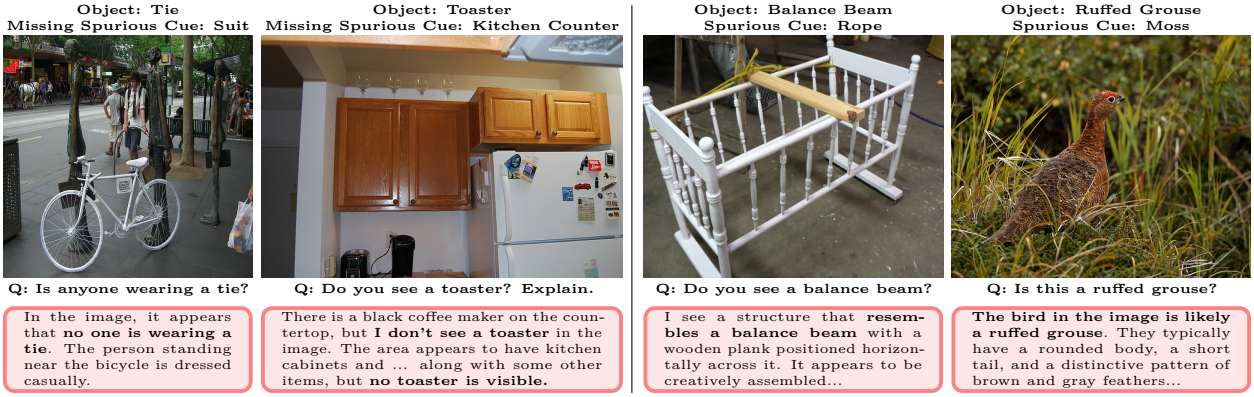

Figure 1: Some failures of GPT-4o-mini identified by *SpurLens*. (**Left**) The model fails to recognize objects in the absence of spurious cues. (**Right**) Spurious cues trigger hallucinations.

these cues. This ranking enables a fine-grained evaluation of how spurious correlations influence both object recognition and hallucination in MLLMs.

Our results reveal that MLLMs over-rely on spurious cues, leading to two major failures. The first is *object recognition* failures: when spurious cues are removed, recognition performance significantly drops. For example, GPT-4o-mini (OpenAI, 2024a) sees a 20.4% accuracy drop on COCO (Lin et al., 2014), from 88.0% to 67.6% (Table 1). The second is *object hallucination*: spurious cues trigger hallucinations, causing models to misidentify objects. For GPT-4o-mini, hallucination rates increase 26-fold when spurious cues are present (Table 2). We illustrate some of these failures in Figure 1.

SpurLens offers three key advantages over prior work. First, *SpurLens* enables the detection of a broader range of spurious cues as it is not limited to predefined features. Second, it provides natural language descriptors for detected cues, offering insight into model biases. Finally, our method requires no human supervision, making it scalable and adaptable across datasets and objects. We validate the reliability and robustness of *SpurLens* through human studies and analysis of its components. Its outputs align closely with human judgments and remain consistent when using different language models to propose spurious cues, highlighting its generality and reproducibility.

While *SpurLens* allows us to systematically analyze spurious correlations in MLLMs, some key questions remain: from where do these biases originate, and can they be mitigated? To address these, we conduct a series of ablation studies designed to isolate different factors contributing to spurious bias. First, we investigate whether spurious bias persists even when all visual evidence of an object is artificially removed by dropping the corresponding visual tokens. We find that even when target objects have been excised from images, MLLMs tend to hallucinate their presence at a high rate. Next, we explore whether alternative prompting strategies can mitigate spurious reliance. We find that prompt ensembling and reasoning-based prompting offer slight situational improvements but do not significantly reduce spurious bias. Even informing the MLLM of spurious features in the prompt does not meaningfully improve performance, indicating that the spurious biases identified by *SpurLens* are fundamental issues. Finally, we examine whether spurious correlations can be measured purely from the MLLM image embeddings. We find that the vision encoder alone also exhibits spurious biases, reinforcing that the issue extends beyond multimodal fusion errors. These findings indicate that spurious bias is a deeply rooted problem in MLLMs and that simple mitigation strategies are insufficient to fully address it.

2 Related Work

Spurious Correlation: Spurious correlations have been extensively studied in the context of deep neural network classifiers (e.g., ViT (Alexey, 2020)), with various approaches proposed to detect and mitigate the issue (Sagawa et al., 2019a; Kirichenko et al., 2022; Noohdani et al., 2024). However, these studies primarily

Figure 2: (**Left**) Object Recognition — the model overrelies on spurious cues for recognition. (**Right**) Object Hallucination — spurious cues amplify hallucinations.

focus on uni-modal settings (image classification tasks). Some research (Wang et al.; Varma et al., 2024; Kim et al., 2023) has explored spurious correlations in CLIP (Radford et al., 2021), framing the problem in terms of zero-shot performance across vision and language modalities. Ye et al. (2024) introduces a visual question answering (VQA) benchmark designed to evaluate MLLMs' reliance on spurious correlations using open-source image datasets. Zheng et al. (2024) also proposes a framework to quantify the varying degrees of robustness of Vision-Language Models (used as few-shot image classifiers) against spurious bias.

Interpretable Spurious Biases: Some works investigate language-interpretable and semi-automatic detection of spurious biases in vision models. Eyuboglu et al. (2022) and Zhang et al. (2023) both identify interpretable high-error slices using cross-modal embeddings; however, the former requires additional feature annotations on each sample, while the latter requires human selection of potential text attributes. Wiles et al. (2023) uses clustering of failure cases and image captioning to identify interpretable spurious features; however, they use image generation models to produce synthetic datasets for iterative refinement. In contrast to these methods, *SpurLens* does not require human supervision, and consistently identifies strong failures in real-world image datasets.

Ranking Images by Spuriosity: One approach to detecting spurious bias in image classifiers is to rank images within their classes based on spuriosity, the degree to which common spurious cues are present. Prior work, such as HardImageNet (Moayeri et al., 2022) and Moayeri et al. (2023), utilized deep neural features from an interpretable network combined with human supervision to identify these cues. In contrast, *SpurLens* eliminates the need for human supervision by leveraging object detectors to automatically rank images based on spurious cues.

Failures of Multimodal Systems: Some studies have introduced frameworks to automatically identify critical shortcomings of MLLMs (Tong et al., 2024a;b). Tong et al. (2024b) highlight MLLMs' struggles with basic visual understanding, attributing these issues to weaknesses in CLIP-based vision encoders. Conversely, Tong et al. (2024a) focuses on the language modality.

Object Hallucination: Object hallucination is an actively studied topic in MLLMs (Hu et al., 2023; Leng et al., 2024; Lovenia et al., 2023; Li et al., 2023; Zhou et al., 2023). POPE (Li et al., 2023) presents the first systematic study on object hallucination in MLLMs, providing an evaluation framework to quantify hallucination. Similarly, Leng et al. (2024) provides additional evidence of object hallucination in MLLMs. Lovenia et al. (2023) argues that hallucination should be distinguished from general incorrectness, introducing a separate benchmark for evaluating object hallucination in MLLMs. Hu et al. (2023) proposes CIEM, an automatic pipeline that leverages an annotated image-text dataset along with an LLM to generate factual and contrastive question-answer pairs for evaluating hallucination in MLLMs. The authors also use CIEM to instruction-tune MLLMs in an attempt to mitigate hallucination. Additionally, Zhou et al. (2023) introduces LURE, a post-hoc method that reduces object hallucination in MLLMs by reconstructing less hallucinatory descriptions. We emphasize that, although our evaluation framework follows POPE (Li et al., 2023) and we adopt the evaluation metrics from Leng et al. (2024), our study is not focused on evaluating object hallucination in MLLMs. The key difference between our work and the studies in this section is that we evaluate the reliance of MLLMs on spurious biases, rather than object hallucination itself.

3 Problem Setting

We briefly present our theoretical framework for studying spurious bias in a multimodal setting. We adopt the common setup described in Ye et al. (2024), where $\mathcal{X}$ and $\mathcal{Y}$ represent the vision and language modalities, respectively. Given an image input $x \in \mathcal{X}$ and a text prompt $y \in \mathcal{Y}$, a MLLM learns the mapping $\phi : \mathcal{X} \times \mathcal{Y} \to \mathcal{O}$ such that $o = \phi(x, y)$, where $o \in \mathcal{O} \subset \mathcal{Y}$ denotes the response.

To study spurious biases, for an object, we define $\mathcal{C} \subset \mathcal{X}$ as the set of images that include target object t, and $\mathcal{S} \subset \mathcal{X}$ as the set of images containing spurious cue f associated with that object. We can partition $\mathcal{X}$ into 4 subsets: Object with Spurious Cue ($\mathcal{C} \cap \mathcal{S}$), Object without Spurious Cue ($\mathcal{C} \cap \mathcal{S}^c$), Spurious Cue without Object ($\mathcal{C}^c \cap \mathcal{S}$), and Baseline (Object and Spurious Cue Free; $\mathcal{C}^c \cap \mathcal{S}^c$). For example, if $t =$"fire hydrant" and $f =$"road", $\mathcal{C}$ is all images including a fire hydrant, and $\mathcal{S}$ is all images including a road. For prompt $y =$"Is there a fire hydrant in the image?", the correct response o is "yes" for $x \in \mathcal{C}$ and "no" for $x \notin \mathcal{C}$. Examples of all four types of images are found in Figure 2.

Note that spurious attributes may also exist in the language modality. In our experiments, we minimize their impact by averaging over multiple simple binary prompts. Moreover, due to the flexibility of language and the extensive amount of text data, spurious attributes in the text modality often exhibit only weak correlations with specific responses, such as "yes" or "no" (Ye et al., 2024).

Similar to Leng et al. (2024), we used two core metrics for our experiments: **Perception Accuracy (PA)** and **Hallucination Rate (HR)**. Formally:

$$\mathbf{PA} := p(o = \text{'yes'} \mid x \in \mathcal{C}, y), \quad \mathbf{HR} := p(o = \text{'yes'} \mid x \in \mathcal{C}^c, y) \tag{1}$$

PA measures the model's ability to accurately perceive objects that are present, and **HR** quantifies the hallucination of non-existent objects. Higher **PA** scores indicate better perception, while lower **HR** scores reflect greater robustness against object hallucinations. To study spurious bias, we analyze how **PA** and **HR** change with and without spurious cues for a given target object t. Formally, for object recognition the Spurious Gap (Moayeri et al., 2023) is defined as $\mathbf{PA\ Gap} := \mathbf{PA}_s - \mathbf{PA}_c$, where:

$$\mathbf{PA}_s := p(o = \text{'yes'} \mid x \in \mathcal{C} \cap \mathcal{S}, y) \qquad \mathbf{PA}_c := p(o = \text{'yes'} \mid x \in \mathcal{C} \cap \mathcal{S}^c, y) \tag{2}$$

Similarly, for object hallucination, the Spurious Gap is defined as $\mathbf{HR\ Gap} := \mathbf{HR}_s - \mathbf{HR}_c$, where:

$$\mathbf{HR}_s := p(o = \text{'yes'} \mid x \in \mathcal{C}^c \cap \mathcal{S}, y) \qquad \mathbf{HR}_c := p(o = \text{'yes'} \mid x \in \mathcal{C}^c \cap \mathcal{S}^c, y) \tag{3}$$

A high Spurious Gap indicates that the MLLM is highly dependent on spurious cues to identify the presence of object t. Appendix B provides further theoretical intuition for these choices of metrics. We believe that modern MLLMs are susceptible to spurious correlations, and thus exhibit high PA and HR Gaps in many cases. We estimate these values by applying selected MLLMs to images from all four partitions of $\mathcal{X}$, once they have been identified.

4 SpurLens: Automating Discovery of Spurious Cues

The spuriosity rankings in HardImageNet (Moayeri et al., 2022; 2023) are constructed using neural features extracted from Salient ImageNet (Singla & Feizi, 2022). This process relies on human supervision to identify spurious features for each class. However, it is limited in scope, detecting only a few spurious features per class. Notably, for nearly two-thirds of ImageNet classes, no spurious cues were detected at all (Moayeri et al., 2023). To study spurious correlations in MLLMs across a broader range of objects and datasets, we develop *SpurLens*, a pipeline designed to produce interpretable spuriosity rankings of images, from which the Spurious Gap can be estimated (outlined in Figure 3).

Suppose that, for a given MLLM $\mathcal{M}$ and target object t, we aim to identify spurious cues for t. Assume that we have access to a large dataset of images, denoted as $\{\mathcal{I}_j\}_{j=1}^N$, and that the presence of t in each image is known; if we are testing object recognition, all images must contain the target object t; if we are testing object hallucination, all images must not contain t.

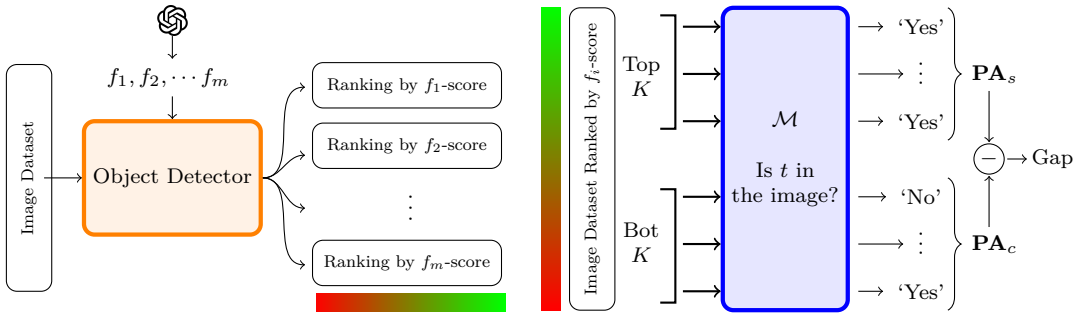

Figure 3: **An overview of** *SpurLens*. **Left**: GPT-4 is used to propose (and filter) spurious features f_i. OWLv2 annotates an image dataset with these spurious features, and its scores are used to rank the image dataset for each feature. **Right**: for a given ranking, the top-K and bottom-K images are passed to an MLLM with a prompt. The responses are aggregated to compute the Spurious Gap.

Proposing Spurious Features We use GPT-4 to generate a list of objects or background elements that commonly appear in images of t. We lemmatize each suggested object, remove duplicates, and remove features that share words with target object name. We then ask GPT-4 several filtering questions to ensure that the proposed objects match the qualifications for being spurious features, and to preemptively eliminate objects that may be challenging for the object detector (e.g., features that are not easily detectable such as "sunlight", or features that are part of the corresponding target object such as "screen" for "laptop"). Note that this filtering reduces the set of potential spurious features in exchange for improved robustness in object detection. See Appendix A for details of these prompts.

Works such as Leng et al. (2024); Zhou et al. (2023); Kim et al. (2024) identify spurious correlations through the frequent co-occurrence of objects in MLLM-generated image captions. Our method avoids this computational cost, and the easily-modifiable prompt structure may suggest a more diverse pool of potential spurious objects.

Identifying Spurious Objects To identify the presence of these spurious features f_i in the images $\mathcal{I}_j$, we use the OWLv2 open-set object detector Minderer et al. (2024). For each image, we query OWLv2 with all potential spurious features and obtain several triplets consisting of a bounding box $b \in [0,1]^4$, label f_i, and confidence score $c \in [0,1]$. Let $\mathcal{O}(\mathcal{I}_i)$ denote the set of such triplets produced by OWLv2 for image $\mathcal{I}_i$. We define the f_i-score of $\mathcal{I}_j$ as

$$S(f_i, \mathcal{I}_j) := \max\left(\{0\} \cup \{c : (b, f_i, c) \in \mathcal{O}(\mathcal{I}_j)\}\right) \tag{4}$$

For each potential spurious feature f_i, we sort the images by f_i-score to obtain a ranking. Validation of object detection results is provided in Appendix F.

Spurious Gaps For each ranking corresponding to feature f_i, let $\mathcal{U}^+_{t,f_i}, \mathcal{U}^-_{t,f_i} \subset \{\mathcal{I}_j\}_{j=1}^N$ be the images with the K-highest and K-lowest f_i-scores respectively. For each of these images, we apply the model $\mathcal{M}$ paired with three prompts $p_k(t)$, $1 \le k \le 3$ (see Appendix A for details). Each prompt asks $\mathcal{M}$ if it sees the target object t in the image, and elicits a Yes/No response; we use three prompts to mitigate the bias due to word choice. We define **PA** (or similarly **HR**) of $\mathcal{M}$ on image $\mathcal{I}$ as:

$$\mathbf{PA}(\mathcal{M}, \mathcal{I}, t) = \frac{1}{3}\sum\nolimits_{k=1}^{3} \mathbb{1}\left(\mathcal{M}(\mathcal{I}, p_k(t)) = \text{"Yes"}\right) \tag{5}$$

We then estimate the Spurious Gap as

$$\mathbf{PA}_s = \frac{1}{K}\sum\nolimits_{\mathcal{I} \in \mathcal{U}^+_{t,f_i}} \mathbf{PA}(\mathcal{M}, \mathcal{I}, t),\ \mathbf{PA}_c = \frac{1}{K}\sum\nolimits_{\mathcal{I} \in \mathcal{U}^-_{t,f_i}} \mathbf{PA}(\mathcal{M}, \mathcal{I}, t),\ \mathbf{PA\ Gap} = \mathbf{PA}_s - \mathbf{PA}_c \tag{6}$$

In the object recognition case, the Spurious Gap measures the difference in recognition accuracy between images with and without f_i, based on the top-K and bottom-K ranked images in the f_i-score ranking. A large positive PA Gap indicates that f_i is truly spurious for t, as the model recognizes t better when the

spurious feature is present. In the object hallucination case, we apply the same methodology but to images that do not contain t. Here, a positive HR Gap means that the model hallucinates the presence of t more frequently when f_i is present, indicating that f_i acts as a spurious cue that triggers hallucination. After computing the Gap for all potential spurious features, we select the feature with the largest Gap as the most influential spurious cue.

Validation In Appendix E, we compare GPT-4's spurious feature proposals with other LLMs (e.g. Gemini) and observe substantial overlap, suggesting that our results are not dependent on the choice of language model. In Appendix I, we study the sensitivity of the computed Gaps to the choice of K, and find that the Gaps stabilize for all models as K increases, indicating the *SpurLens* results are robust to this parameter. In Appendix F, we assess the accuracy of the OWLv2 object detector with two human studies. First, we randomly sample detection outputs and check whether human annotators agree with the presence/absence of the spurious cue in the top- and bottom-ranked images; we find high agreement: 93% on COCO and 90% on ImageNet. Second, we for a random subset of spurious cues identified by *SpurLens*, we replace the object detector results with human annotations, and compute Gaps based on the human-labeled top- and bottom-ranked images; we observe strong alignment with the *SpurLens* gaps. This demonstrates that, while the object detector may itself be subject to some spurious biases, our methodology is sufficiently robust to enable reliable detection of large spurious gaps. In Appendix N, we compare *SpurLens* gaps to a random baseline, providing evidence that the signals *SpurLens* detects are statistically significant.

Finally, we note that *SpurLens* emphasizes precision, rather than recall or completeness: it aims to consistently and robustly find strong spurious cues, rather than the absolute best cue for each model and dataset. While our results cannot be used to directly compare models, we do find significant spurious biases in all models that we evaluate. Although *SpurLens* uses binary-resemblance prompts to evaluate MLLMs (for ease of evaluation and minimizing other sources of bias), we find many instances of the identified biases manifesting in open-ended generation (see Appendices C, D, and R).

5 Results

Models For our experiments, we evaluate three open-source MLLMs, Qwen2-VL-7B-Instruct (Wang et al., 2024), Llama-3.2-11B-Vision-Instruct (Meta, 2024), and LLaVA-v1.6-mistral-7B (Liu et al., 2023), along with one closed-source model, GPT-4o-mini (OpenAI, 2024a).

Datasets We use three image datasets in our evaluation: HardImageNet (Moayeri et al., 2022), ImageNet (Russakovsky et al., 2015), and COCO (Lin et al., 2014). To maintain comparability with prior work, we use a subset of 100 classes from ImageNet as chosen in Spurious ImageNet (Neuhaus et al., 2023). These datasets offer diverse visual contexts, enabling analysis of spurious correlations across different domains. They also vary in complexity: HardImageNet is curated to highlight spurious correlations, while COCO contains diverse real-world scenes, providing a broader evaluation of MLLM robustness. In contrast, older benchmarks such as CelebA (Liu et al., 2015) and Waterbirds (Sagawa et al., 2019b) were designed for unimodal classifiers trained end-to-end, and thus fail to challenge MLLMs in a zero-shot setting. See Appendices G and H for further discussion.

Evaluation For each class in all three datasets, we initially generate 32 potential spurious features, which are then passed through various filters (see Appendix A). We compute the PA/HR Gap for each feature, and choose the most influential one as the *SpurLens* feature for that class. For each dataset, we take the class-wise average of the chosen PA/HR Gaps and report the final aggregated metrics.

5.1 Object Recognition

The results are presented in Table 1. We use $K = 50$ for HardImageNet and the ImageNet subset, and $K = 100$ for COCO. We observe that performance decreases across all models when spurious cues are absent, with the magnitude of this drop varying between models and datasets. Some qualitative examples of GPT-4o-mini failures are provided in Appendix D. Additional qualitative examples are found in Appendix R, which compares the behavior of open-source models with and without spurious cues. While the models

Table 1: **Object Recognition.** Perception Accuracy (PA%) across different datasets and models. PA_s and PA_c are accuracy on high-spurious and spurious-free images. Results are averaged over classes.

Dataset	**HardImageNet**			**ImageNet Subset**			**COCO**		
Model	PA_s	PA_c	Gap	PA_s	PA_c	Gap	PA_s	PA_c	Gap
Qwen2-VL	99.3	93.4	5.9	98.4	91.7	6.7	95.3	80.1	15.2
Llama-3.2	93.1	78.1	15.0	90.6	72.9	17.7	95.0	80.0	14.8
LLaVA-v1.6	96.0	82.8	13.2	93.0	77.3	15.7	95.6	79.6	16.0
GPT-4o-mini	95.0	82.4	12.6	95.7	83.8	11.9	88.0	67.6	20.4

generate detailed and accurate descriptions when spurious cues are present, the descriptions become less accurate when they are absent.

We conduct a class-wise analysis of spurious bias: the distribution of PA across ImageNet and COCO classes for Qwen2-VL (Wang et al., 2024) is visualized in Figure 5 (see Appendix Q for other models). When spurious cues are absent, accuracy decreases and variance increases, indicating that models struggle to generalize without these cues. The distributions also confirm that spurious bias is highly class-dependent. We provide a detailed breakdown of the strongest spurious cues and their corresponding Spurious Gaps as identified by *SpurLens*, for each model and class, in Appendix S.

5.2 Object Hallucination

We visualize an example of a spurious cue leading to hallucination, as identified by *SpurLens*, in Figure 4. Given an MLLM and a large image dataset, *SpurLens* detects the most influential spurious cues based on their Spurious Gap. For LLaVA (Liu et al., 2024a) with target object "bird", *SpurLens* identifies "feeder" as the most influential spurious cue. In Figure 4, we demonstrate that this cue can indeed trigger hallucinations in the model. We provide more qualitative examples in Appendix C.

Recall that to compute HR Gaps with *SpurLens*, for each class we require an image dataset that does not contain the target object. COCO is a large-scale object segmentation dataset, whose 80 categories are grouped into 10 supercategories. For each target object, we run *SpurLens* on images from the same supercategory that do not contain the target object. We exclude three COCO classes (keyboard, dining table, and sports ball) from our final analysis because these objects frequently appear in the dataset without being annotated, making HR measurements unreliable for these categories. For ImageNet, for each of the 100 classes, we randomly sample 5,000 images outside of the class to serve as our dataset. We compute rankings with $K = 50$ for ImageNet and $K = 100$ for COCO. As an ablation, we provide an alternative setup using these two datasets in Appendix L.

The quantitative results are presented in Table 2. We observe that for both COCO and ImageNet, the hallucination rate is significantly higher when spurious cues are present. In COCO, the class-wise averaged HR is at least 5 times higher in high-spurious images across all models; the effect is more pronounced in ImageNet, with it being at least 18 times higher. These results demonstrate that spurious bias makes MLLMs vulnerable to hallucination, as models fail to distinguish between true object presence and misleading contextual cues.

Similar to PA, we conduct a class-wise analysis, to examine hallucination across objects. The distribution of HR for Qwen2-VL is visualized in Figure 5 (see Appendix Q for other models). When spurious cues are present, hallucinations become significantly more pronounced. HR varies across classes, indicating that some objects are more susceptible to hallucination than others. We provide detailed class-wise results, in Appendix S.

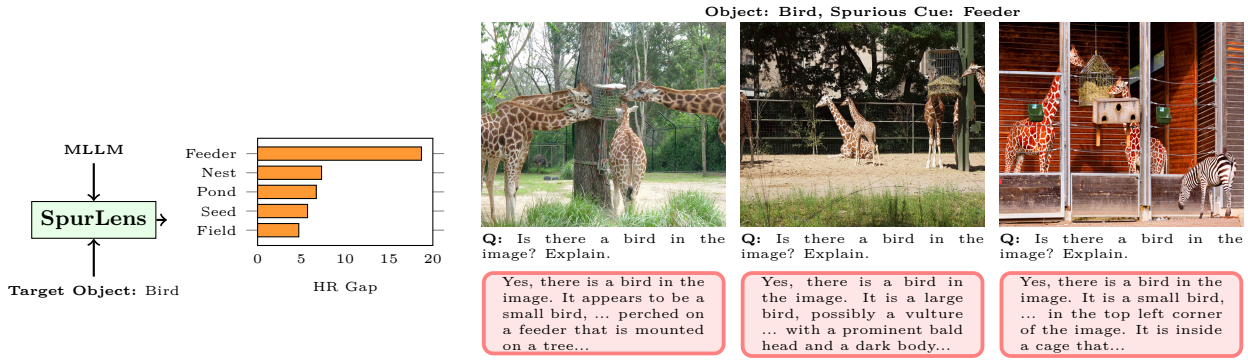

Figure 4: An example hallucination identified by *SpurLens*: (**Left**) *SpurLens* ranks the most influential spurious cues. (**Right**) The spurious cue, 'feeder' in this case, triggers hallucination in the model.

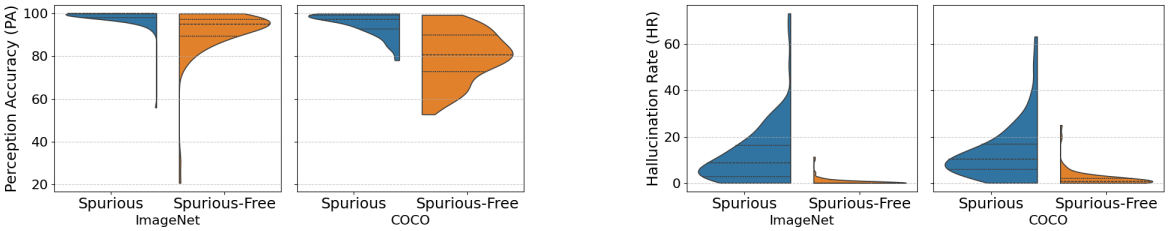

Figure 5: Per-class PA and HR distributions for Qwen2-VL across two datasets.

6 Ablation Studies

6.1 Dropping Visual Cues

Both HardImageNet (Moayeri et al., 2022) and COCO (Lin et al., 2014) have pixel-level mask annotation of the target object. We leverage these to create artificial negative samples by removing visual cues of the target object and and evaluate to what extent the models hallucinate their presence.

All open-source MLLMs have a vision encoder that patchifies the image, tokenizes each patch, and processes the resulting visual tokens. We drop the tokens associated with the target object before they are processed by the vision encoder (Jain et al., 2022). Since different MLLMs have varying architectures, we implement this token-dropping approach separately for each model; see Appendix K for implementation details. We also test hallucination rates on blank (fully black) images, where all visual cues are removed.

The results for this experiment are shown in Table 3. We observe significantly higher HR rates compared to Table 2. This poor performance likely arises because these images are out-of-distribution (OOD) samples, making them more challenging for the models. However, even under these OOD conditions, we observe that HR remains higher when spurious cues are present, reinforcing that models strongly rely on spurious correlations when the target object is absent. We also find that HR_b, the hallucination rate on blank (fully black) images, is not always zero, meaning some models hallucinate objects even when given a completely blank input. This highlights that spurious bias in MLLMs is not solely dependent on visual features.

6.2 Mitigation

SpurLens is developed as a diagnostic tool that automatically identifies interpretable causes of spurious bias, which can be used for mitigation. However, in this section, we establish that the spurious biases identified are a fundamental issue and cannot be trivially overcome through language-based techniques. We focus on Chain-of-Thought (CoT) prompting, which encourages language models to generate rationales for their solution to a base prompt. Zero-shot CoT has previously been shown to improve performance on various

Table 2: Hallucination rates (HR %) for high-spurious vs spurious-free images. When spurious cues are present, hallucination rates increase.

Model	ImageNet Subset			COCO		
	HR_s	HR_c	Gap	HR_s	HR_c	Gap
Qwen2-VL	12.1	0.5	11.6	13.5	1.8	11.7
Llama-3.2	9.0	0.5	8.6	18.1	3.8	14.4
LLaVA-v1.6	18.4	1.0	17.4	21.8	2.7	19.2
GPT-4o-mini	5.2	0.2	5.1	11.2	1.4	9.8

Table 3: Hallucination rates (HR %) after object token-dropping. Models hallucinate even when target object features are removed.

Model	HardImageNet			COCO		
	HR_s	HR_c	HR_b	HR_s	HR_c	HR_b
Qwen2-VL	50.2	37.2	6.6	35.3	15.1	5.5
Llama-3.2	31.5	20.4	4.9	34.8	15.1	4.0
LLaVA-1.6	45.7	34.6	0.0	40.0	16.4	0.0

benchmarks in both textual and multimodal scenarios (Wei et al., 2023; Kojima et al., 2022; Luo et al., 2024; Zhang et al., 2024).

We evaluate five strategies. (1) Prompt Ensembling, where we take the majority vote among multiple queries with different prompt phrasing. (2) Dual Prompting, where we first ask for a general image description before prompting for object recognition. (3) Guiding Prompting, where we explicitly instruct the model to focus on key details and avoid misleading background cues. (4) Spurious List, where we provide the model with a list of potential spurious features (the list of GPT-4 suggested features that *SpurLens* analyzes). (5) Spurious Top, where we provide the model with the strongest spurious feature as identified by *SpurLens* (note that this is improper, as it incorporates *SpurLens*' knowledge of the full dataset). The prompts used in these strategies are provided in Appendix A.

The results are provided in Table 4. PA is evaluated on HardImageNet, while HR is evaluated on Spurious ImageNet (Neuhaus et al., 2023). While the ensemble/reasoning-based strategies offer slight improvements on certain models and metrics, none of the strategies perform significantly better or have substantially smaller Spurious Gap compared to the baseline. The Spurious Top strategy "cheats" compared to the other strategies by using *SpurLens*' analysis and identification of the strongest spurious cue on each class' dataset, which is the same dataset the model is being evaluated on; yet, it also does not perform well relatively. Further discussion of these strategies and their relative performance can be found in Appendix J. The continued presence of the Spurious Gap across all strategies suggests that language-based methods, while influencing the model's behavior, cannot eliminate the underlying reliance on spurious cues; Spurious Gaps detected by *SpurLens* are a more fundamental issue that cannot be resolved solely through prompting techniques.

6.3 Examining Spuriousity in the Vision Encoder

As suggested in Tong et al. (2024a;b), MLLMs' poor performance on perception tasks may be attributed to poor information or visual ambiguity in the vision encoder features. To study this, we train binary classifiers on vision encoder features and perform the same experiments as before to compute Spurious Gaps for HardImageNet classes. By isolating the vision encoder, we ablate away any biases that could come from the language model component.

For each image in HardImageNet, we obtain a vector by averaging the embeddings of all image patches. For each class, we train a logistic regression binary classifier that determines whether a given embedding is of an image from that class. We evaluate the bias of this classifier by computing the PA Gap with the K most and least-spurious images of that class. This experiment is done for various compositions and sizes of the training dataset; further details and results are found in Appendix M.

The results in this simple setting reaffirm key observations from our main experiments. The spurious biases measured from these linear classifiers are of similar magnitude to those measured from the Qwen2-VL experiments ($\sim 6\%$ class-wise average PA Gap). This suggests the vision embeddings are affected by spurious bias, and that language supervision did not significantly effect our main experimental results. While the training dataset size and composition for the linear classifiers effected the size of the Gap, spurious bias was

Table 4: **Mitigation Attempt via Prompting.** Perception Accuracy (PA%) and Hallucination Rate (HR%) across different prompting strategies and models. The Spurious Gap persists in all strategies.

Model	Metric	Baseline	Ensemble	Guiding	Dual	Spur. List	Spur. Top
Qwen2	PA_s	98.1	**98.5**	97.5	95.2	96.5	97.0
	PA_c	91.9	**92.4**	89.3	82.3	85.9	88.9
	HR_s	9.5	8.6	16.4	**4.0**	5.5	4.8
	HR_c	1.2	1.0	0.8	**0.4**	0.5	0.8
	HR_b	3.3	**0**	**0**	**0**	**0**	1.0
Llama	PA_s	95.1	**96.8**	95.6	95.2	73.3	95.2
	PA_c	84.7	**87.0**	**87.0**	84.4	63.2	85.6
	HR_s	11.0	**7.5**	15.1	7.6	4.8	10.3
	HR_c	2.2	1.5	4.1	3.1	**1.0**	2.0
	HR_b	7.0	**0**	4.7	**0**	0.7	0.6
LLaVA	PA_s	91.4	92.4	**99.2**	89.3	94.8	89.6
	PA_c	85.2	86.4	**91.2**	72.0	81.2	82.7
	HR_s	12.5	11.0	24.6	**5.6**	11.1	9.5
	HR_c	2.1	1.9	5.8	**0.8**	1.6	1.4
	HR_b	**0**	**0**	**0**	**0**	**0**	**0**

still present and significant in all cases. Finally, the magnitude of spurious bias is highly class-dependent, which affirms our distributional analysis of the effect.

7 Conclusion

We present *SpurLens*: an adaptable, automated, and interpretable system for identifying spurious cues for objects. We use *SpurLens* to find spurious cues for ImageNet and COCO classes and quantitatively evaluate the Spurious Gaps caused by the presence/absence of these features for several MLLMs. Our findings show that modern MLLMs are still highly susceptible to spurious correlations. We hope that our process to discover and measure spurious biases guides future developments for effective mitigation and downstream tasks dependent on accurate visual perception.

Limitations. Our method assumes that the image dataset being studied is reasonably large and diverse, so that many of the spurious features proposed appear often enough to be evaluated. Filtering the set of proposed spurious features helped to minimize errors in object detection, although it likely decreased the maximum spurious gaps we could measure. While the method is computationally efficient, scaling linearly with dataset size, runtime may become a bottleneck for very large datasets. Finally, *SpurLens* is diagnostic in nature: it reveals when and where models rely on spurious cues but does not identify their root causes or a robust mitigation strategy; this is an avenue for future work.

Reproducibility Statement. All of the open-source models referenced in Section 5 were accessed through HuggingFace. The prompts used for generating the potential spurious features, filtering, and evaluating MLLMs is found in Appendix A. The *SpurLens* code used to generate and evaluate spurious features is submitted as supplementary material, and will be made publicly available and linked in the camera-ready version.

References

Dosovitskiy Alexey. An image is worth 16x16 words: Transformers for image recognition at scale. *arXiv preprint arXiv: 2010.11929*, 2020.

Tianheng Cheng, Lin Song, Yixiao Ge, Wenyu Liu, Xinggang Wang, and Ying Shan. Yolo-world: Real-time open-vocabulary object detection, 2024. URL `https://arxiv.org/abs/2401.17270`.

Sabri Eyuboglu, Maya Varma, Khaled Saab, Jean-Benoit Delbrouck, Christopher Lee-Messer, Jared Dunnmon, James Zou, and Christopher Ré. Domino: Discovering systematic errors with cross-modal embeddings, 2022. URL https://arxiv.org/abs/2203.14960.

Hongyu Hu, Jiyuan Zhang, Minyi Zhao, and Zhenbang Sun. Ciem: Contrastive instruction evaluation method for better instruction tuning. *arXiv preprint arXiv:2309.02301*, 2023.

Saachi Jain, Hadi Salman, Eric Wong, Pengchuan Zhang, Vibhav Vineet, Sai Vemprala, and Aleksander Madry. Missingness bias in model debugging. In *International Conference on Learning Representations*, 2022. URL https://openreview.net/forum?id=Te5ytkqsnl.

Jae Myung Kim, A Koepke, Cordelia Schmid, and Zeynep Akata. Exposing and mitigating spurious correlations for cross-modal retrieval. In *Proceedings of the IEEE/CVF Conference on Computer Vision and Pattern Recognition*, pp. 2585–2595, 2023.

Younghyun Kim, Sangwoo Mo, Minkyu Kim, Kyungmin Lee, Jaeho Lee, and Jinwoo Shin. Discovering and mitigating visual biases through keyword explanation, 2024. URL https://arxiv.org/abs/2301.11104.

Polina Kirichenko, Pavel Izmailov, and Andrew Gordon Wilson. Last layer re-training is sufficient for robustness to spurious correlations. *arXiv preprint arXiv:2204.02937*, 2022.

Takeshi Kojima, Shixiang Shane Gu, Machel Reid, Yutaka Matsuo, and Yusuke Iwasawa. Large language models are zero-shot reasoners. *Advances in neural information processing systems*, 35:22199–22213, 2022.

Sicong Leng, Yun Xing, Zesen Cheng, Yang Zhou, Hang Zhang, Xin Li, Deli Zhao, Shijian Lu, Chunyan Miao, and Lidong Bing. The curse of multi-modalities: Evaluating hallucinations of large multimodal models across language, visual, and audio. *arXiv preprint arXiv:2410.12787*, 2024.

Yifan Li, Yifan Du, Kun Zhou, Jinpeng Wang, Wayne Xin Zhao, and Ji-Rong Wen. Evaluating object hallucination in large vision-language models. *arXiv preprint arXiv:2305.10355*, 2023.

Tsung-Yi Lin, Michael Maire, Serge Belongie, James Hays, Pietro Perona, Deva Ramanan, Piotr Dollár, and C Lawrence Zitnick. Microsoft coco: Common objects in context. In *Computer Vision–ECCV 2014: 13th European Conference, Zurich, Switzerland, September 6-12, 2014, Proceedings, Part V 13*, pp. 740–755. Springer, 2014.

Haotian Liu, Chunyuan Li, Yuheng Li, and Yong Jae Lee. Improved baselines with visual instruction tuning, 2023.

Haotian Liu, Chunyuan Li, Yuheng Li, Bo Li, Yuanhan Zhang, Sheng Shen, and Yong Jae Lee. Llava-next: Improved reasoning, ocr, and world knowledge, January 2024a. URL https://llava-vl.github.io/blog/2024-01-30-llava-next/.

Shilong Liu, Zhaoyang Zeng, Tianhe Ren, Feng Li, Hao Zhang, Jie Yang, Qing Jiang, Chunyuan Li, Jianwei Yang, Hang Su, Jun Zhu, and Lei Zhang. Grounding dino: Marrying dino with grounded pre-training for open-set object detection, 2024b. URL https://arxiv.org/abs/2303.05499.

Ziwei Liu, Ping Luo, Xiaogang Wang, and Xiaoou Tang. Deep learning face attributes in the wild. In *Proceedings of International Conference on Computer Vision (ICCV)*, December 2015.

Holy Lovenia, Wenliang Dai, Samuel Cahyawijaya, Ziwei Ji, and Pascale Fung. Negative object presence evaluation (nope) to measure object hallucination in vision-language models. *arXiv preprint arXiv:2310.05338*, 2023.

Xuewen Luo, Fan Ding, Yinsheng Song, Xiaofeng Zhang, and Junnyong Loo. Pkrd-cot: A unified chain-of-thought prompting for multi-modal large language models in autonomous driving, 2024. URL https://arxiv.org/abs/2412.02025.

Meta. Llama-3.2-11b-vision-instruct, 2024. URL https://huggingface.co/meta-llama/Llama-3.2-11B-Vision-Instruct. Accessed: 2025-01-14.

Matthias Minderer, Alexey Gritsenko, and Neil Houlsby. Scaling open-vocabulary object detection, 2024. URL https://arxiv.org/abs/2306.09683.

Mazda Moayeri, Sahil Singla, and Soheil Feizi. Hard imagenet: Segmentations for objects with strong spurious cues, June 2022.

Mazda Moayeri, Wenxiao Wang, Sahil Singla, and Soheil Feizi. Spuriosity rankings: sorting data to measure and mitigate biases. *Advances in Neural Information Processing Systems*, 36:41572–41600, 2023.

Yannic Neuhaus, Maximilian Augustin, Valentyn Boreiko, and Matthias Hein. Spurious features everywhere-large-scale detection of harmful spurious features in imagenet. In *Proceedings of the IEEE/CVF International Conference on Computer Vision*, pp. 20235–20246, 2023.

Fahimeh Hosseini Noohdani, Parsa Hosseini, Aryan Yazdan Parast, Hamidreza Yaghoubi Araghi, and Mahdieh Soleymani Baghshah. Decompose-and-compose: A compositional approach to mitigating spurious correlation. In *Proceedings of the IEEE/CVF Conference on Computer Vision and Pattern Recognition*, pp. 27662–27671, 2024.

OpenAI. Gpt-4o mini: Advancing cost-efficient intelligence, 2024a. URL https://openai.com/index/gpt-4o-mini-advancing-cost-efficient-intelligence/. Accessed: 2025-01-14.

OpenAI. Gpt-4 technical report, 2024b. URL https://arxiv.org/abs/2303.08774.

Alec Radford, Jong Wook Kim, Chris Hallacy, Aditya Ramesh, Gabriel Goh, Sandhini Agarwal, Girish Sastry, Amanda Askell, Pamela Mishkin, Jack Clark, et al. Learning transferable visual models from natural language supervision. In *International conference on machine learning*, pp. 8748–8763. PMLR, 2021.

Olga Russakovsky, Jia Deng, Hao Su, Jonathan Krause, Sanjeev Satheesh, Sean Ma, Zhiheng Huang, Andrej Karpathy, Aditya Khosla, Michael Bernstein, et al. Imagenet large scale visual recognition challenge. *International journal of computer vision*, 115:211–252, 2015.

Shiori Sagawa, Pang Wei Koh, Tatsunori B Hashimoto, and Percy Liang. Distributionally robust neural networks for group shifts: On the importance of regularization for worst-case generalization. *arXiv preprint arXiv:1911.08731*, 2019a.

Shiori Sagawa, Pang Wei Koh, Tatsunori B Hashimoto, and Percy Liang. Distributionally robust neural networks for group shifts: On the importance of regularization for worst-case generalization. *arXiv preprint arXiv:1911.08731*, 2019b.

Sahil Singla and Soheil Feizi. Salient imagenet: How to discover spurious features in deep learning?, 2022. URL https://arxiv.org/abs/2110.04301.

Shengbang Tong, Erik Jones, and Jacob Steinhardt. Mass-producing failures of multimodal systems with language models. *Advances in Neural Information Processing Systems*, 36, 2024a.

Shengbang Tong, Zhuang Liu, Yuexiang Zhai, Yi Ma, Yann LeCun, and Saining Xie. Eyes wide shut? exploring the visual shortcomings of multimodal llms. In *Proceedings of the IEEE/CVF Conference on Computer Vision and Pattern Recognition*, pp. 9568–9578, 2024b.

Hugo Touvron, Louis Martin, Kevin Stone, Peter Albert, Amjad Almahairi, Yasmine Babaei, Nikolay Bashlykov, Soumya Batra, Prajjwal Bhargava, Shruti Bhosale, et al. Llama 2: Open foundation and fine-tuned chat models. *arXiv preprint arXiv:2307.09288*, 2023.

Maya Varma, Jean-Benoit Delbrouck, Zhihong Chen, Akshay Chaudhari, and Curtis Langlotz. Ravl: Discovering and mitigating spurious correlations in fine-tuned vision-language models. *arXiv preprint arXiv:2411.04097*, 2024.

Peng Wang, Shuai Bai, Sinan Tan, Shijie Wang, Zhihao Fan, Jinze Bai, Keqin Chen, Xuejing Liu, Jialin Wang, Wenbin Ge, Yang Fan, Kai Dang, Mengfei Du, Xuancheng Ren, Rui Men, Dayiheng Liu, Chang Zhou, Jingren Zhou, and Junyang Lin. Qwen2-vl: Enhancing vision-language model's perception of the world at any resolution. *arXiv preprint arXiv:2409.12191*, 2024.

Qizhou Wang, Yong Lin, Yongqiang Chen, Ludwig Schmidt, Bo Han, and Tong Zhang. A sober look at the robustness of clips to spurious features. In *The Thirty-eighth Annual Conference on Neural Information Processing Systems*.

Jason Wei, Xuezhi Wang, Dale Schuurmans, Maarten Bosma, Brian Ichter, Fei Xia, Ed Chi, Quoc Le, and Denny Zhou. Chain-of-thought prompting elicits reasoning in large language models, 2023. URL https://arxiv.org/abs/2201.11903.

Olivia Wiles, Isabela Albuquerque, and Sven Gowal. Discovering bugs in vision models using off-the-shelf image generation and captioning, 2023. URL https://arxiv.org/abs/2208.08831.

Wenqian Ye, Guangtao Zheng, Yunsheng Ma, Xu Cao, Bolin Lai, James M Rehg, and Aidong Zhang. Mm-spubench: Towards better understanding of spurious biases in multimodal llms. *arXiv preprint arXiv:2406.17126*, 2024.

Yuhui Zhang, Jeff Z. HaoChen, Shih-Cheng Huang, Kuan-Chieh Wang, James Zou, and Serena Yeung. Diagnosing and rectifying vision models using language, 2023. URL https://arxiv.org/abs/2302.04269.

Zhuosheng Zhang, Aston Zhang, Mu Li, Hai Zhao, George Karypis, and Alex Smola. Multimodal chain-of-thought reasoning in language models, 2024. URL https://arxiv.org/abs/2302.00923.

Guangtao Zheng, Wenqian Ye, and Aidong Zhang. Benchmarking spurious bias in few-shot image classifiers. In *European Conference on Computer Vision*, pp. 346–364. Springer, 2024.

Yiyang Zhou, Chenhang Cui, Jaehong Yoon, Linjun Zhang, Zhun Deng, Chelsea Finn, Mohit Bansal, and Huaxiu Yao. Analyzing and mitigating object hallucination in large vision-language models. *arXiv preprint arXiv:2310.00754*, 2023.

A Prompts

A.1 Evaluation

We used the following three prompts for our main experiments when querying the MLLMs.

Prompts to Evaluate Perception/Hallucination for an Image

- Do you see a CLASSNAME in the image? Answer with 'Yes' or 'No'.
- Is there a CLASSNAME in the image? Answer with 'Yes' or 'No'.
- Determine whether there is a CLASSNAME in the image. Reply with 'Yes' or 'No'.

The following prompts were used in Section 6.2.

Prompting Strategies

Ensemble: We performed a majority vote among the following prompts:
1) Do you see a CLASSNAME in the image? Answer with 'Yes' or 'No'.
2) Is there a CLASSNAME in the image? Answer with 'Yes' or 'No'.
3) Determine whether there is a CLASSNAME in the image. Reply with 'Yes' or 'No'.

Guiding:
Do you see a CLASSNAME in the image? Describe all objects in the image. Pay attention to key details that confirm their presence. Be mindful of misleading background features, but do not ignore real objects. Finally, answer with 'Yes' or 'No'.

Dual: We first ask the model for a general image description before prompting for object detection

1. Describe the most prominent objects in this image.
2. Is there a CLASSNAME in the image? Answer with 'Yes' or 'No'.

Spurious List: Do you see a CLASSNAME in the image? Describe all objects in the image. Pay attention to key details that confirm their presence. Be mindful of misleading background features, but do not ignore real objects. For example, spurious cues like CUES_LIST may appear but are not directly related to the CLASSNAME. Focus on distinguishing the CLASSNAME from such irrelevant features. Finally, answer with 'Yes' or 'No'.

Spurious Top: Is there a CLASSNAME in the image? Be aware that the presence or absence of a STRONGEST_CUE does not necessarily indicate the presence or absence of a CLASSNAME. Answer with 'Yes' or 'No'.

A.2 Feature Generation

We used the following prompts with GPT-4 to generate potential spurious features for a given class.

Generating Potential Spurious Features

The prompts began with one of the following two options:

- "List N objects that commonly appear in images of a CLASSNAME."
- "List N background elements that commonly appear in images of a CLASSNAME."

To each of these was appended:
"The objects cannot be part of a CLASSNAME. List exactly one item on a every consecutive line, followed by a period and a one sentence explanation. The object must be physical and discernable in an image. The object name must be less than two words. Do not number the responses. Do not output anything else."

We used several prompts with GPT-4 to filter the proposed spurious features, keeping only those features which get the desired answer for all questions. We provide all our prompts below.

Filtering Prompts

- "Can a FEATURENAME exist without a CLASSNAME?" (Desired answer: "Yes".)
- "Is a FEATURENAME part of a CLASSNAME?" (Desired answer: "No".)
- "Do all or almost all FEATURENAME have a CLASSNAME?" (Desired answer: "No".)
- "Do all or almost all CLASSNAME have a FEATURENAME?" (Desired answer: "No".)

Now we eliminate objects that may be challenging for the object detector (for example, features that are not easily detectable such as "sunlight", or features that are physically part of the corresponding target object such as "screen" for "laptop"). We use the following prompts for this matter.

Filtering Prompts: Detectability

Determine whether the provided object or feature is visualizeable in an image. An object is visualizeable in an image if the object has a physical presence, and it is always clear what pixels in the image comprise the specific object. Be conservative when labeling a feature as not detectable; only do so if you are completely sure. Respond with 'Yes' or 'No' only.

Here are some example responses:
'sunlight': No
'trail': Yes
'walk': No
'fluoride': No
'toothpaste': Yes
'algae': No
'water': Yes

Determine whether the following object or feature is visualizeable:

'SPUR FEATURE':

Filtering Prompts: Vocabulary

Determine whether the meaning of the provided feature might be too difficult most people to understand without background context. A feature is too difficult if the feature is too niche to a specific context, is very uncommon, or has an unusual spelling. Be conservative in labelling a feature as too difficult; only do so when you are completely sure that most people would not know the correct meaning without additional information. Respond with 'Yes' or 'No' only.

Here are some examples:
'saddle': No
'equine': Yes
'grille': Yes
'trunk': No
'liana': Yes
'vine': No

Determine whether the following feature is too difficult:

'SPUR FEATURE':

Filtering Prompts: Synonyms

Determine whether two objects provided are synonyms of each other, or instances of each other. This is not asking whether the two objects are similar. Only answer 'Yes' if the two terms generally refer to the same object. Respond with 'Yes' or 'No' only.

Here are some examples:
'car', 'vehicle': Yes
'truck', 'bumper': No
'surfboard', 'skimboard': Yes
'remote', 'game controller': Yes
'motorcycle', 'bike': Yes
'motorcycle', 'pedal': No
'cradle', 'rocker': Yes
'bed', 'sleeping mat': Yes
'laptop', 'tablet': No
'backpack', 'purse': No

Determine whether the following two objects are synonyms or instances of each other:

'SPUR FEATURE', 'TARGET OBJECT':

Filtering Prompts: Separable

Determine whether the two objects provided are inseparable from each other. Answer 'Yes' one of the objects is part of the other, or if they are nearly always found together. This is not asking whether the two objects are similar or related. Only answer 'Yes' if most people could not distinguish between the two objects when shown an example, or whether it is almost impossible to find one object without the other. Respond with 'Yes' or 'No' only.

Here are some examples:
'cell phone', 'screen': Yes
'ski', 'snowboard': No
'bed', 'nightlight': No
'oven', 'stove': Yes
'boat', 'anchor': Yes
'canoe', 'sail': No
'train', 'railroad': Yes
'train', 'traffic signal': No

Determine whether the following two objects are inseparable from each other:

'SPUR FEATURE', 'TARGET OBJECT':

Filtering Prompts: Composition

Determine whether the first object is part of the second object. Respond with 'Yes' if the first object is frequently physically attached to the second object, refers to some component of the second object, or is a property of the second object. This is not asking whether the two objects are similar or often seen together. Only answer 'Yes' if you generally cannot have the second object without the first object. Respond with 'Yes' or 'No' only.
Here are some examples:
'power cord', 'hair dryer': Yes
'bookmark', 'book': No
'handlebar', 'bicycle': Yes
'label', 'wine bottle': Yes
'collar', 'dog': No
'drinking glass', 'wine bottle': No
'soil', 'plant pot': Yes
'rod', 'pull-up bar': Yes

Answer for the following object or term.

'SPUR FEATURE', 'TARGET OBJECT':

Filtering Prompts: Confusion

Determine whether an instance of the first object in a photograph could be easily confused as being the second object type. This is not asking whether the two objects are similar or often seen together. Only answer 'Yes' if the two objects look so similar to each other that most people would not be able to tell the difference between them in an image when viewed from certain angles. Respond with 'Yes' or 'No' only.

Here are some examples:
'knife', 'fork': Yes
'chopstick', 'fork': No
'balloon', 'kite': Yes
'airplane', 'kite': No
'parking space', 'parking meter': No
'parking space', 'parking lot': Yes
'coffee cup', 'cup', : Yes
'straw', 'cup': No
'juice', 'cider': Yes
'barrel', 'composter': Yes
'soil', 'mulch': Yes
'double bass', 'guitar': No

Answer for the following object or term.

'SPUR FEATURE', 'TARGET OBJECT':

B Theoretical Intuition for Gap Metrics

B.1 Perception Accuracy

Our notion of multimodal spurious bias can be considered a relaxation of the framework proposed in Ye et al. (2024); using our notation,

$$p(o = \text{“yes"} \mid x \in \mathcal{C} \cap \mathcal{S}, y) \gg p(o = \text{“yes"} \mid x \in \mathcal{C}, y) \tag{7}$$

Our definition of **PA Gap** $= \mathbf{PA}_s - \mathbf{PA}_c$ from Equation 2 is related to Equation 7 by the law of total probability. To illustrate this, let $\alpha = p(x \in S^c \mid x \in \mathcal{C}, y)$. We derive the relationship as follows:

$$\mathbf{PA}_s - \mathbf{PA} = \mathbf{PA}_s - \alpha\mathbf{PA}_c - (1-\alpha)\mathbf{PA}_s = \alpha(\mathbf{PA}_s - \mathbf{PA}_c) \tag{8}$$

Thus, the **Spurious Gap** represents the multimodal spurious bias, scaled by $\frac{1}{\alpha}$. Note that α reflects the strength of the spurious correlation. If the spurious cue is almost always present when the object is present, α would approach zero, resulting in the Spurious Gap being much larger than the bias.

B.2 Object Hallucination

Define $\beta = p(x \in S \mid x \in \mathcal{C}^c, y)$. From definition of **HR** and using the law of total probability, we derive:

$$\mathbf{HR} = (1-\beta)\mathbf{HR}_c + \beta\mathbf{HR}_s \tag{9}$$

We argue that β is near zero because the set $\mathcal{C}^c$ is much larger than $\mathcal{S}$. Additionally, we assume that the model is resistant to object hallucination on baseline images. This assumption is based on the fact that, among the four subsets partitioning $\mathcal{X}$, baseline is the largest. Formally, $\mathbf{HR}_c \approx 0$. Our empirical evidence supports this assumption. Combining these two assumptions with Equation 9, we obtain:

$$\frac{1}{\beta}\mathbf{HR} \approx \mathbf{HR}_s \tag{10}$$

Equation 10 demonstrates that even though the general hallucination rate for a model might be low, the presence of spurious cues can amplify it significantly on a large scale.

C Qualitative Examples of Object Hallucination

We provided some of the hallucinations identified by *SpurLens* in Figure 6 and Figure 7.

D Qualitative Examples of GPT-4o-mini Spurious Gap

We provided some of the object recognition failures identified by *SpurLens* in Figure 8.

E Consistency Across Feature-Proposal LLMs

SpurLens relies on GPT-4 for generating spurious features for each target object. Our usage of this particular model may incur some bias in what features are proposed, or which target objects get better-aligned features for object detection and recognition tasks. To study this, we experiment with feature generation on two additional LLMs: Qwen2.5 72B, and Gemini 2.5 Flash.

For both the 15 HardImageNet classes and the 79 COCO classes, we generate potential spurious features with both LLMs using the same method as described in Section 4. We use the same prompts to generate the base list of features, and perform basic de-duplication, lemmatization, and filtering using the 4 prompts that determine whether the proposed object follows the definition of a "spurious feature". However, we do not perform the extensive filtering with the prompts that utilize in-context examples, as we wish to study the distribution of features proposed without concern for the object detector.

To compare the lists of features generated by these two alternative LLMs with those generated by GPT-4, we utilize semantic similarity matching. For each dataset class, we take the list $\{f_i\}_{i=1}^{n}$ generated by GPT-4 and the list $\{\tilde{f}_j\}_{j=1}^{m}$ generated by the alternative LLM, and compute the pair-wise similarity as the cosine similarity of embeddings using the all-MiniLM-L6-v2 embedding model. For each feature proposed by the alternative LLM, we select highest similarity with respect to all GPT-4 proposed features:

$$S(\tilde{f}_j) = \max_i \cos(f_i, \tilde{f}_j)$$

We wish to examine the distribution of this value within a class. We introduce a thresholded metric, the "proposal similarity at α", defined as the proportion of features for which the S-value is at least α:

$$\text{PS}_\alpha = \frac{1}{m} \sum_{j=1}^{m} \mathbb{1}\left(S(\tilde{f}_j) > \alpha\right)$$

Empirically, we find that a similarity score above $\alpha = 0.7$ means that the two features are extremely similar apart from some adjective (for example, $\cos(\text{"trees"}, \text{"pine trees"} = 0.7994)$, and a similarity score above $\alpha = 0.5$ means that the objects are similar in subject and closely related. We compute values of $\text{PS}_{0.7}$ and $\text{PS}_{0.5}$ for both alternative LLMs, for all HardImagNet and COCO classes. We summarize the class-wise averaged results in Table 5. This demonstrates significant similarity in the features proposed by the alternative LLMs with those proposed by GPT-4o. The significant overlap we find with other LLMs shows that using GPT-4o does not introduce significant bias in our methodology. Further, since *SpurLens* focuses on precision rather than recall, the diversity of generations is a more significant factor, and is demonstrated to be adequate for this application.

F Human Study Validation

We conduct two human studies to validate the precision and reliability of the rankings produced by *SpurLens*.

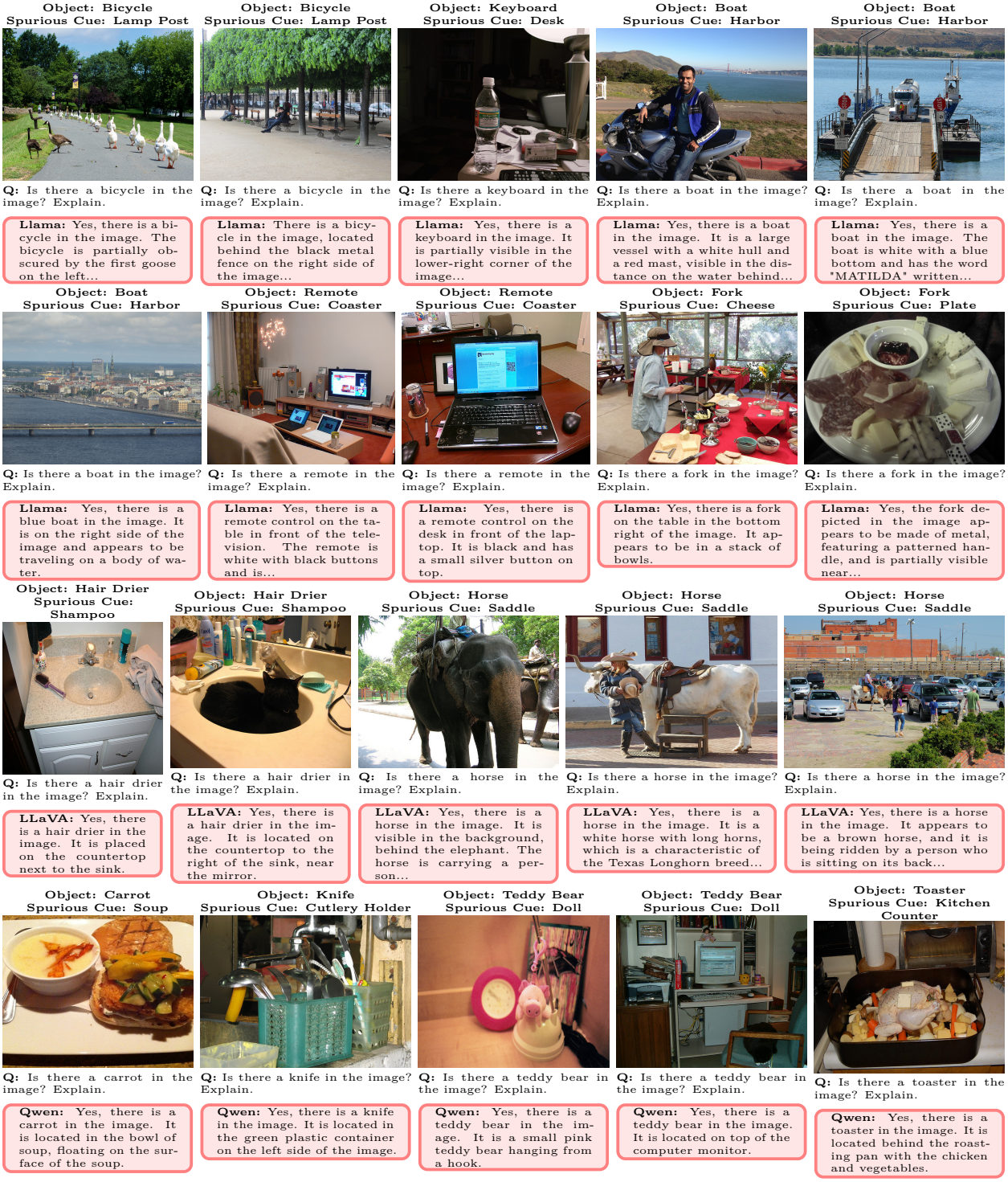

Figure 6: Hallucinations identified by *SpurLens*, part 1

F.1 Agreement with Object Detector

In the first study, we evaluate the quality of the spurious cue detection step. For a randomly selected subset of classes (20 from COCO and 25 from ImageNet), we asked human annotators to label whether the spurious cue was present in the top 10 and bottom 10 images ranked by *SpurLens*. We then compute agreement between

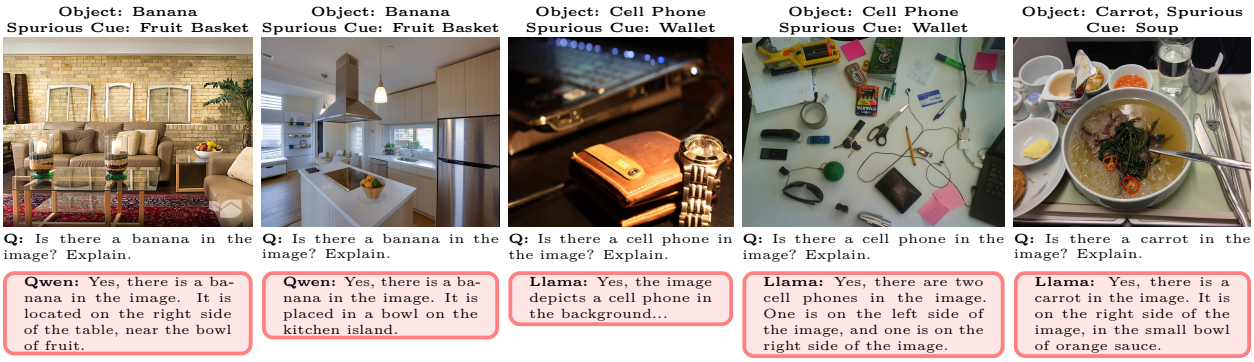

Figure 7: Hallucinations identified by *SpurLens*, part 2

Figure 8: Some failures of GPT-4o-mini (accessed in March 2025) on COCO object perception tasks when spurious features are *not* present.

the object detector and human judgments. As shown in Table 6, human agreement is high, suggesting that OWLv2 reliably distinguishes the presence or absence of cues in most cases.

To provide qualitative support, we also visualize example detections. We randomly selected 4 COCO classes and uniformly sampled images from the top- and bottom-ranked sets (based on cue presence) from one of the *SpurLens* rankings. Example detections are shown in Figure 10.

Table 5: Metrics describing the similarity of features proposed by alternative LLMs compared with those generated with GPT-4. All numbers are averaged class-wise. For both models, nearly half of the features are near-equivalent, and the majority are very similar.

Dataset	**HardImageNet**		**COCO**	
Model	$PS_{0.7}$	$PS_{0.5}$	$PS_{0.7}$	$PS_{0.5}$
Gemini 2.5 Flash	52.4	67.0	42.9	61.9
Qwen 2.5 72B	49.2	69.4	42.0	62.9

Qwen 2.5 72B	GPT-4o	Gemini 2.5 Flash
water	water	water
rain	rain	rain
cloud	cloud	cloud
bird	bird	bird
leaf	leaf	leaf
fruit	fruit	fruit
flower	flower	flower
branch	tree branch	branch
insect	insect	insect
tree	tree	tree
sunlight	sunlight	forest
moss	moss	sunlight
soil	fallen logs	sun
butterfly	sky	log
grass	nest	sky
vine	liana	nest
fern	rock	liana
egg	vine	rock
feather	nut	vine
sloth	underbrush	nut
snake	shade	air
dirt	fallen leaves	soil
	stream	canopy
	banana	dirt
	bark	mud
	foliage	
	bamboo	
	coconut	

Figure 9: Spurious features proposed for HardImagNet class “howler monkey” by Qwen2.5 72B, GPT-4o, and Gemini 2.5 Flash.

It is worth noting that we also experimented with using Grounding DINO (Liu et al., 2024b) as an open-set object detector in place of OWLv2. However, we found that its detections were qualitatively less consistent and reliable. As a result, we use OWLv2 exclusively in our pipeline.

F.2 Agreement on Spurious Gap

In the second study, we assess whether the gaps computed by *SpurLens* align with those derived from human-annotated spurious cues. We randomly sampled 20 object-cue pairs from COCO and asked human annotators to label whether the associated spurious feature was present in each image. Using these annotations, we recompute the PA Spurious Gap with $K = 50$, and compare it to the gap produced by *SpurLens* using

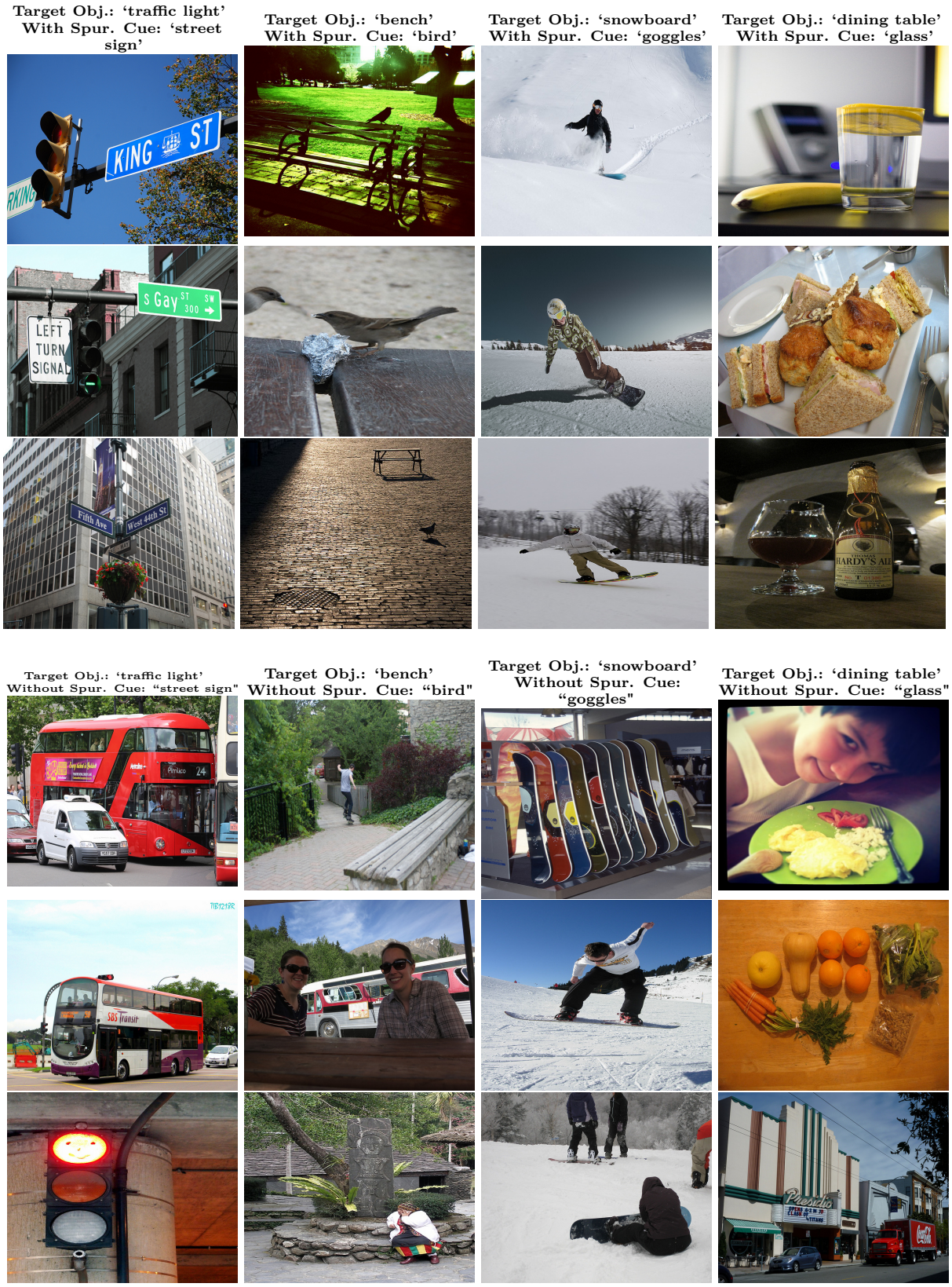

Figure 10: For the randomly-chosen COCO classes 'traffic light' (10), 'bench' (15), 'snowboard' (36), and 'dining table' (67), we randomly choose one of the spurious features we evaluated, and then randomly chose images from the top-100 and bottom-100 in the object detection ranking for that class/feature pair.

Table 6: Human agreement with object detector results on top/bottom 10 ranked images across 20 (COCO) and 25 (ImageNet) randomly selected classes.

Dataset	Top Agreement	Bottom Agreement	Average
COCO	0.89	0.96	0.925
ImageNet	0.84	0.948	0.894

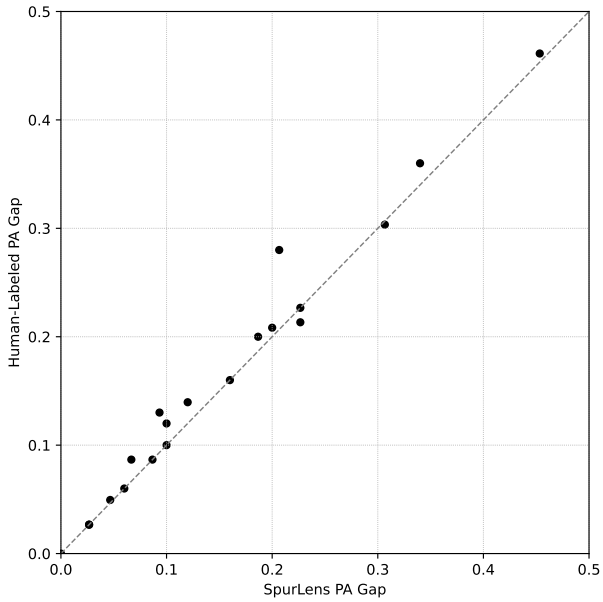

Figure 11: Comparison of SpurLens PA Gap and human-labeled PA Gap (both computed with $K = 50$) across 20 COCO classes. The strong correlation (Pearson $r = 0.988$) indicates that SpurLens produces rankings consistent with human judgments.

the same K. As shown in Figure 11, the two sets of gap values are highly correlated (Pearson $r = 0.988$), supporting the claim that *SpurLens* produces human-aligned and reliable rankings.

G CelebA Evaluation

While *SpurLens* focuses on spurious biases related to object recognition and hallucination, prior work has extensively studied other forms of bias, such as correlations between gender and blond hair in the CelebA (Liu et al., 2015) dataset, particularly in unimodal classification settings (Noohdani et al., 2024; Sagawa et al., 2019a; Kirichenko et al., 2022). Following this line of work, we examine whether such spurious correlations persist in MLLMs.

We adopt a similar evaluation setup: using the prompt "Does the person in the image have blond hair? Answer with 'Yes' or 'No'," we measure accuracy across groups with and without the spurious feature (gender). Results are shown in Table 7. While Spurious Gap still exists, we argue that it is not particularly meaningful in this context. In prior work, Unimodal classifiers trained with ERM performed poorly on the worst group (e.g., blond males), often below 50%. In contrast, MLLMs like Qwen2-VL achieve over 96% accuracy on this group in a zero-shot setting. Moreover, the CelebA annotations are noisy, and in many cases where Qwen's predictions differ from the labels, the true hair color is ambiguous even to humans. Figure 12 shows qualitative examples.

Table 7: Qwen2-VL accuracy on CelebA across gender and hair color. The spurious feature in this setting is gender. All numbers are percentages.

Hair Color	**Male**	**Female**	**Gap**
Blond	96.63	98.28	1.65
Non-blond	81.70	74.84	6.86

Figure 12: Qualitative examples from CelebA where Qwen-VL's answer ("Not blond") differs from the annotated ground truth ("Blond"). Hair color is often ambiguous, even for humans.

H Waterbirds Evaluation

Similar to CelebA, the Waterbirds dataset has often been used to study the effect of spurious correlations in vision classifiers. Unlike CelebA, however, it is a synthetic dataset with a simplified structure. This may pose issues for MLLMs, which may err due to the synthetic, out-of-distribution nature of the inputs rather than the spurious correlations. As our goal is to draw conclusion about the performance of modern MLLMs in practical, real-world settings, the results of such an analysis may not be fully applicable.

Additionally, Waterbirds was designed for evaluating spurious correlations in a training setup. In the training phase, the dataset creates strong spurious cues (e.g., landbirds predominantly being on land and waterbirds on water). This creates a high spurious correlation that the model learns to rely on. However, during testing, the dataset balances these cues, which causes a drop in classifier accuracy. In contrast, our work focuses on a zero-shot setup, where the model is not explicitly trained on such cues, and any spurious correlations that arise are more naturally occurring. Thus, we believe evaluating on such a synthetic, domain-specific setup would not align with the goal of evaluating MLLMs in more complex, real-world scenarios.

Nevertheless, we still explore Waterbirds' applicability within the context of MLLMs. We use the following prompt: "We call a bird 'waterbird' if it is a seabird (albatross, auklet, cormorant, frigatebird, fulmar, gull, jaeger, kittiwake, pelican, puffin, or tern) or waterfowl (gadwall, grebe, mallard, merganser, guillemot, or Pacific loon). Is there a waterbird in the image? Answer with 'Yes' or 'No'." This prompt is similar to our standard prompts, prepended by a definition of the target class "waterbird" (following the definition provided by Sagawa et al. (2019a)). The results are presented in Table 8. We observe that all MLLMs examined still exhibited significant spurious gaps, which we interpret as a clear indicator of residual spurious correlations in the models.

Table 8: Accuracy of various open-source models on Waterbirds. All numbers are percentages.

Model	**Waterbird (Water)**	**Waterbird (Land)**	**Landbird (Water)**	**Landbird (Land)**
Qwen	94.58	81.35	64.02	96.03
LLaVA	59.33	13.24	77.38	99.76
Llama	94.34	79.90	38.99	70.88

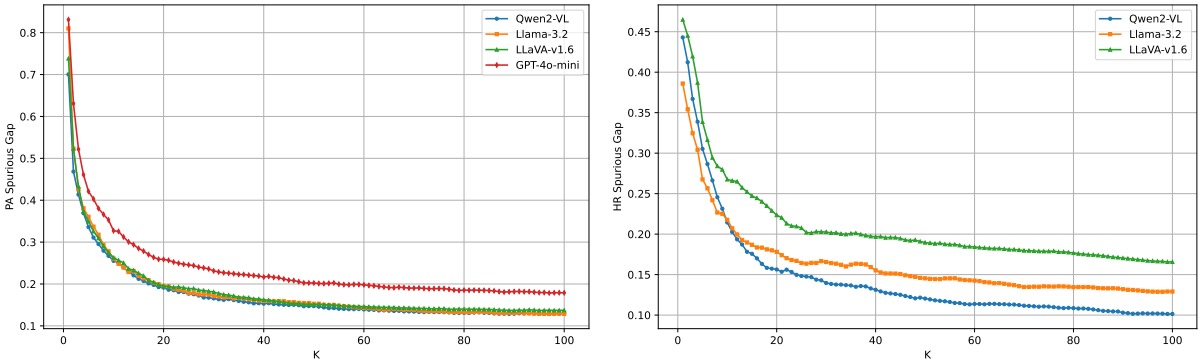

Figure 13: PA (**Left**) and HR (**Right**) Spurious Gap as a function of K, the number of top/bottom images used in evaluation. Gaps stabilize for $K \sim 60$, suggesting robustness to this parameter.

I Hyperparameter Sensitivity Analysis

We study how the Spurious Gap varies with the hyperparameter K, which controls the number of top- and bottom-ranked images used to compute the gap. As shown in Figure 13, all models exhibit a similar trend: the Spurious Gap decreases for larger values of K and stabilizes as K increases. This behavior is expected: smaller K focuses on more extreme samples and amplifies the gap, while larger K smooths the estimate by averaging over a broader set of images.

Importantly, the gap values begin to stabilize around $K \approx 60$, indicating that *SpurLens* produces consistent rankings and that our reported gaps are not highly sensitive to this parameter. These trends support the robustness of our method and suggest that our main findings are not artifacts of a specific K choice.

J Prompting Mitigation Discussion

This is an extended discussion of the attempted prompt-based mitigation from Section 6.2.

Table 4 includes HR_b: the hallucination rates on blank (fully black) images. While HR_b is not always zero in the Baseline setting, it drops to zero with Ensemble or Dual Prompting, suggesting that these strategies help suppress some hallucinations.

The results in Table 4 reveal a trade-off between accuracy and hallucination rates across the reasoning-oriented strategies. Dual Prompting reduces HR, but at the cost of lower PA, while Guiding Prompting improves PA but increases hallucinations, suggesting that encouraging the model to focus on key details might reinforce reliance on spurious cues. In contrast, Prompt Ensembling provides a minor but consistent improvement across all cases, reducing HR while slightly increasing PA, making it the most balanced strategy. None of these increases or decreases are very significant, and none of these strategies resolve the Spurious Gap.

The final two strategies, Spurious List and Spurious Top, aim to leverage the textual information retrieved by the *SpurLens* pipeline. Since SpurLens leverages LLMs to identify spurious biases in natural language for each class, a natural idea is to provide a list of such potential features to the examined LLMs, which may cause them to recognize and/or avoid the bias; this is the basis of the Spurious List strategy. After running the *SpurLens* pipeline, we know which of the proposed spurious features is strongest for each class. Providing only this feature (rather than the list of all features, not all of which may be spurious) is not proper, as it contains information from the entire class dataset upon which we are also evaluating. Nevertheless, even with this additional information, we find that spurious bias still clearly persists. In fact, the results for the Spurious List and Spurious Top strategies are often weaker than the reasoning and ensembling-based strategies

The Spurious Gap remains present across all prompting strategies, suggesting that while prompt engineering can influence model behavior, it does not eliminate the underlying reliance on spurious cues. This indicates

that the Spurious Gaps detected by *SpurLens* are a more fundamental issue that cannot be resolved solely through prompting techniques.

K Token Dropping

K.1 Implementation

We implemented token-dropping for Qwen2-VL, Llama-3.2 11B Vision Instruction, and LLaVa 1.6. We will focus on Qwen2-VL, as the discussion for the other models is roughly similar.

Suppose that we have an image of a target object, and have a bitmask of the object for that image. We aim to drop visual tokens from Qwen2-VL's processing of the image, without affecting its vision of other areas. After some basic resizing, Qwen2-VL breaks the image into patches of size 14×14 pixels. However, adjacent 2×2 tokens are later merged into a single token by a simple MLP layer (Wang et al., 2024). Therefore, when dropping tokens, we must effectively work with a "token size" of 28×28 pixels.

For a given mask/image pair, after reshaping the mask in the same way that Qwen does, we condense the mask into a boolean for each 14×14 pixel patch, where a patch is `false` if any part of the mask lies within the 28×28 pixel area of the token that the patch is a part of, and `true` otherwise. (This is essentially flood-filling the the inverted mask into 28×28 pixel regions, then extracting all 14×14 chunks as booleans.) This condensed mask is then passed through the model into the vision encoder, where it is used to index the patch embeddings such that only the patches outside the expanded mask are kept. The mask indexing is also applied to the rotary positional embeddings, before both the positional and patch embeddings are passed to the patch-to-token merger. The mask information is also be passed to the input processor in order to add the correct number of vision placeholder tokens for the image.

(a) (b) (c) (d)

Figure 14: An example for token-dropping. (a) shows the original figure of a howler monkey, and (b) shows the mask of this image from HardImageNet. (c) Illustrates the regions that are dropped by token-dropping. In (d), the areas of the image that will be dropped are corrupted with uniform random noise.

Figure 14 illustrates the procedure using an image/mask pair from the "howler monkey" class of HardImageNet. Figure 14 (a) and (b) show the image and mask, and (c) shows the regions of the image that would be dropped, which is a superset of the mask. (Note that we visualize this as a mask, but the model would not see black masked-out regions – the tokens for those regions would not be present at all.)

K.2 Validation

We devise a small demonstration to show the validity of our method: we pass images to Qwen2-VL with the prompt "Is something wrong with this image?". The responses with various images from Figure 14 are as follows:

- With original image (a): "The image appears to be a close-up of tree branches and leaves. There doesn't seem to be anything inherently wrong with the image; it's a natural scene."
- With the masked image (b): "Yes, there appears to be an issue with the image. The silhouette of the animal seems to be floating in the air without any visible connection to the tree branches or

Table 9: Comparison of HR Gaps (as %) on artificial negative samples from HardImageNet. The Gaps are computed with $K = 50$, and the class-wise average is reported.

Model	**Token-Dropping**			**Masking**		
	HR_s	HR_c	HR Gap	HR_s	HR_c	HR Gap
Qwen2-VL	50.2	37.2	13.0	53.1	35.7	17.4
Llama-3.2	31.5	20.4	11.1	44.0	27.3	16.7
LLaVA-1.6	45.7	34.6	11.1	40.5	31.3	9.2

leaves. This suggests that the image might be digitally altered or manipulated, as it is not a natural occurrence for an animal to be floating in the air without support."

- With the token-dropped image (visualized as a mask in (c)): "The image appears to be a close-up of tree branches and leaves. There doesn't seem to be anything inherently wrong with the image; it's a natural scene."
- We add uniform random noise to the area of the image that will be dropped to obtain (d). We then pass in the corrupted image with the same tokens dropped as in (c). The model answers: "The image appears to be a close-up of tree branches and leaves. There doesn't seem to be anything inherently wrong with the image; it's a natural scene."

The model does not notice any irregularities in the image in the token-dropping scenario, and further does not notice any noise corruption under the area that is dropped, confirming that the model does not see the dropped regions at all.

K.3 Comparison with Masking

In Section 6.1, we computed HR Gaps on HardImageNet classes, using token-dropping to create artificial samples without the target object. Here, we compare those results to the results if we were to use masking (filling in the masked area with 0 RGB pixel values) to create the artificial negative samples.

The results are in Table 9. We find relatively similar class-wise averaged performance between the two constructions. Both methods give very large HR estimates, likely because both are out-of-distribution (OOD) images. Nevertheless, the HR Gap in both scenarios provides additional evidence of spurious correlation effects.

L Spurious Bias in MLLMs: Evidence Without *SpurLens*

In this section, we provide evidence that spurious bias in MLLMs can be observed even without using *SpurLens*. Instead of systematically identifying high-spurious images, we leverage existing benchmarks, Spurious ImageNet (Neuhaus et al., 2023) and COCO (Lin et al., 2014), to demonstrate this issue.

Spurious ImageNet is a subset of 100 classes from ImageNet (Russakovsky et al., 2015), containing 75 images per class that include spurious cues but lack the target object. For baseline images, we randomly selected 75 images from ImageNet for each class.

COCO is a large-scale object detection, segmentation, and captioning dataset with rich annotations. It includes 80 categories organized into 10 supercategories (e.g., kitchen, furniture, vehicle). We argue that using only supercategory annotations is sufficient to support our claims. For each category, we randomly selected 500 images from the same supercategory but belonging to different categories as our spurious images. Additionally, we selected 500 images from different supercategories as spurious cue-free images.

We illustrate some hallucinations produced by GPT-4o-mini in this setup in Figure 16. The quantitative results for this experiment are shown in Table 10. For COCO, even with our simple setup for identifying spurious images, the HR is at least three times higher than that of the baseline images. For Spurious

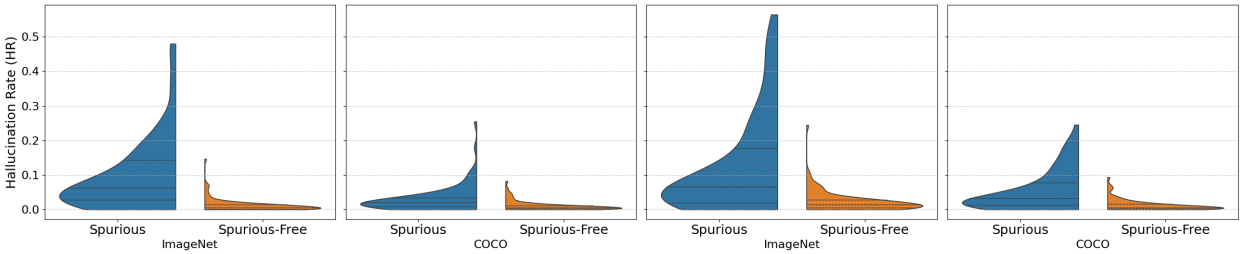

Figure 15: The distribution of HR across Spurious ImageNet and COCO classes for (**Left**) Qwen2-VL and (**Right**) LLaVA-v1.6. When spurious cues are present, hallucination amplifies.

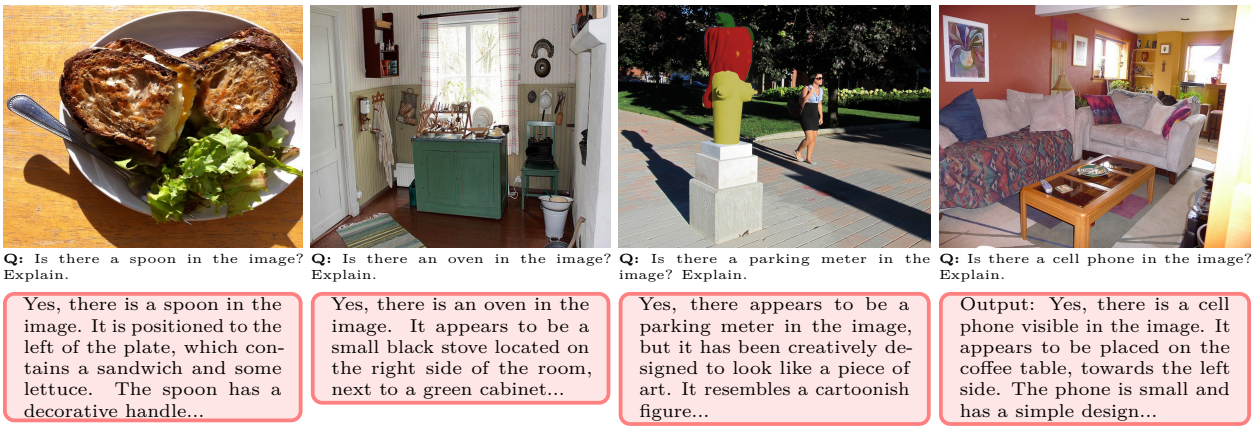

Figure 16: Some failures of GPT-4o (accessed in January 2025) identified by our method. The model hallucinates when spurious cues are present.

ImageNet, which systematically identifies spurious cues for each class, the ratios are even larger. Additionally, we visualized the HR distribution across different classes in Figure 15. Our findings align with Moayeri et al. (2023), highlighting that the bias from reliance on spurious cues is critically class-dependent.

Table 10: Hallucination Rates (HR) for Spurious ImageNet and COCO datasets. When spurious cues are present, the hallucination rate increases by at least threefold. * indicates that for GPT, due to API costs, we selected 100 images from COCO per category, compared to 500 images for other models.

Model	**Spurious ImageNet**		**COCO**	
	HR_s	HR_c	HR_s	HR_c
Qwen2-VL	**9.5**	1.1	**3.1**	1.0
Llama-3.2	**11.0**	2.1	**9.6**	3.1
LLaVA-v1.6	**12.5**	2.2	**5.5**	1.2
GPT-4o-mini	**3.2**	0.3	**2.6***	0.5*

M Vision Encoder Experiments

To further analyze the problem of spurious correlations, we perform a similar analysis to the main paper in a highly simplified setting, and show that several intuitions and results discussed hold true. We focus on the Qwen2-VL vision encoder, train various binary linear classifiers on HardImageNet data, and demonstrate that the effect of spurious correlations can still be found.

First, for each image in HardImageNet-train, we use the Qwen2-VL vision encoder to get the embedding for each 14×14 token in the image. We average the embeddings of all tokens to get a single representative embedding (vector of length 3584) for each image.

For each HardImageNet class, we train a logistic regression binary classifiers to determine whether a given image embedding is of that class. Let the target class be $c \in [1, 15]$. Consider the embeddings from HardImageNet-train of class c; after removing the $K = 100$ least spurious and $K = 100$ most spurious images (according to the original HardImageNet ranking), we randomly sample x of the remaining images as the positive examples in our training dataset (where x variable). For the negative examples in the training dataset, we randomly sample $f \times x$ embeddings from HardImageNet-train excluding class c (where $f \geq 1$ is variable). This construction of the dataset allows us to control (1) the scale of the training dataset through x, and (2) how unbalanced the dataset is through f (the positive:negative sample ratio in the training dataset is $1 : f$).

After training the logistic regression classifier on this dataset, we estimate the PA Gap $= \mathrm{PA}_s - \mathrm{PA}_c$ as before by computing the accuracy on the $K = 100$ most spurious and $K = 100$ least spurious images in HardImageNet-train of class c (note that these were excluded from the training dataset). Additionally, we run the classifier on all of HardImageNet-val to get a better understanding of its overall accuracy.

Because the training datasets are randomly sampled, for each value of x and f and class c, we train 10 such classifiers with this procedure and average the results for PA_s, PA_c, the PA Gap, and the HardImageNet-val accuracies. This experiment is performed for $x \in \{100, 200, \ldots 600\}$ and $f \in \{1, 2, 3, 5, 7\}$.

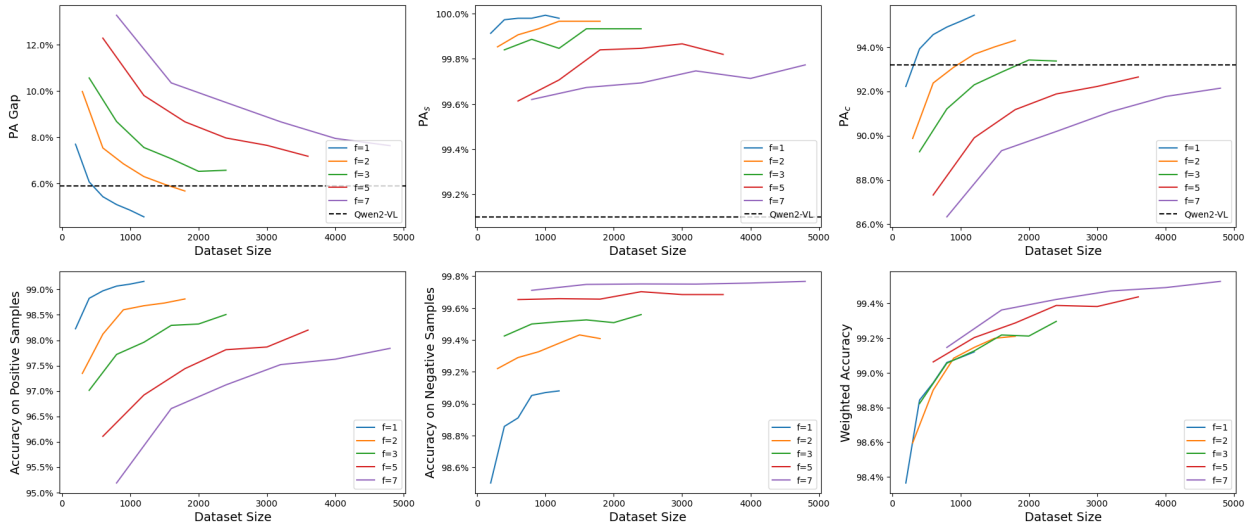

Figure 17: PA Gap results for various binary linear classifiers trained on mean-pooled image embeddings. The plots show various dataset sizes and levels of sample balance; each point is the classwise average (over 15 HardImageNet classes) of the metric shown; the metric for each class is the average of the results of 10 experiments on random training datasets, as previously described. The PA Gap (top left) is the difference between PA_s (top middle) and PA_c (top right). Accuracies are evaluated on HardImageNet-val on the target class (bottom left) and all classes except the target class (bottom middle). The weighted accuracy (bottom-right) is a 1:f weighted average of these two. For the top three images, the PA values for Qwen2-VL from the main experiments are also depicted for comparison.

The (class-wise averaged) results for the PA metrics are found in Figure 17. Note that the training dataset size (horizontal axis) is computed as $x \times (1 + f)$. There are a few point to note. First, the classwise-averaged PA Gap measured for Qwen2-VL in our main experiments is of similar magnitude to the PA Gaps measured for these binary classifiers, which indicates that the vision encoder is largely responsible for spurious bias effect and that the language model component did not significantly influence our results. Second, increasing dataset size tends to improve accuracy on both positive and negative samples, increase perception accuracy

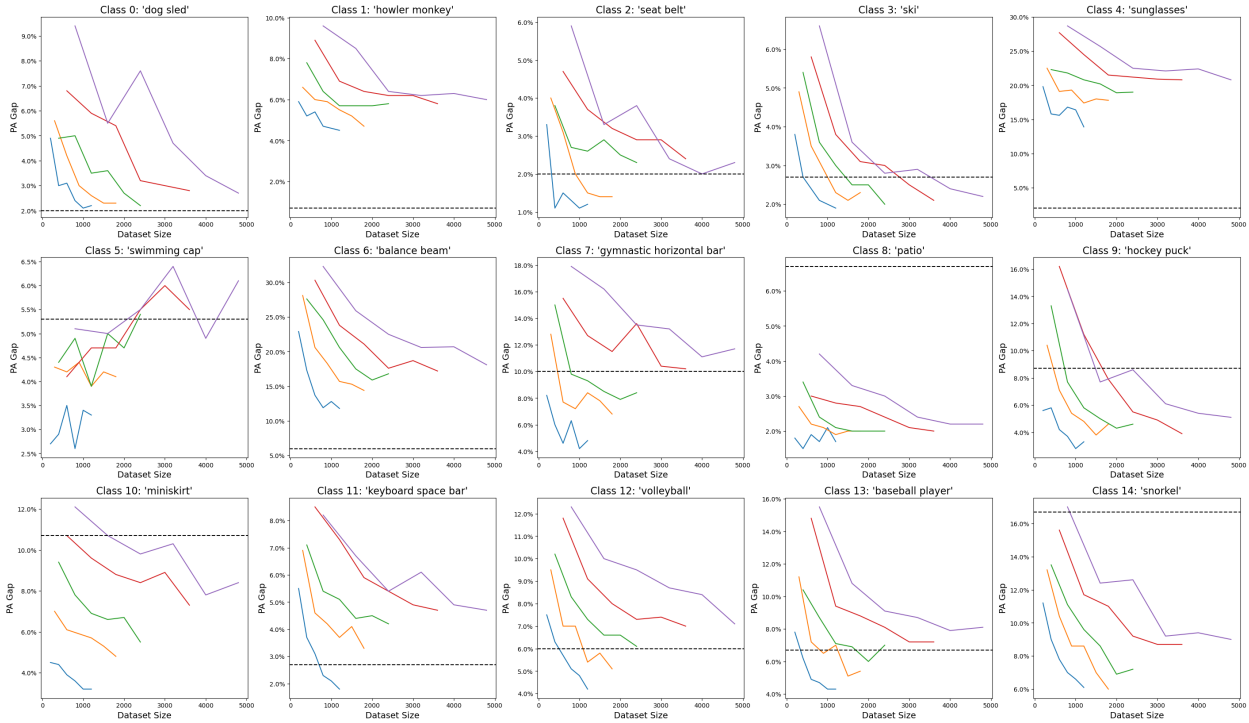

Figure 18: PA Gaps separately for each HardImageNet class for all experiments in Figure 17. The colors for different values of f are the same as in that figure.

for both spurious and non-spurious images, and decreases the spurious gap; this is fairly intuitive. Third, for more unbalanced training datasets (larger values of f), the accuracy on positive samples tends to be lower, which is expected in a binary classification problem. However, the figure shows that in evaluating PA, there are far more errors for non-spurious images than there are for spurious images. When the model has seen a very wide set of images (which is true in the case of MLLMs), images without spurious features tend to be misclassified much more often than high-spurious images. This suggests that the source of spurious bias lies within the image embedding being insufficient to robustly distinguish between classes.

While the trends are somewhat clear for class-wise averaged results, there is significant variation between classes. Figure 18 presents the results of the experiments for each class separately. We see a significant variation in the scale of PA Gap as well as in the level of decrease in PA Gap as dataset size increases. Thus, while the effects discussed are generally true, the impact of spurious correlations in the image embeddings on perception is highly class-dependent.

Finally, we directly compare the gaps obtained through these vision encoder logistic regressions with the PA gaps from evaluation on Qwen2-VL on the HardImageNet rankings. Using $f = 7$, $K = 50$, and taking the maximum possible value of x for each dataset (that being $2K$ less than the size of the HardImageNet-train for that class), we obtain a PA Gap on the vision encoder logistic regression classifier for each HardImageNet class. The class-wise average of these gaps is 0.082. Comparing these gaps class-wise against the PA Gaps obtained when evaluating Qwen2-VL on the HardImageNet rankings (with $K = 50$), we find a linear correlation coefficient of 0.25. This suggests that the vision encoder is partially responsible for the observed spurious bias in the full MLLM.

N SpurLens Validation

We apply SpurLens to the 15 HardImageNet classes. As discussed in Section 4, we use GPT-4 to generate 32 potential spurious features for each class, which are subsequently filtered through GPT filters and manual

review of object detector results. For each model, after computing the PA Gap (with $K = 50$) for each potential spurious feature , we select the feature with the largest PA gap as the PA gap for the class; we then average these results class-wise.

We compare the PA Gaps of the spurious ranking selected by SpurLens to the PA Gap (with $K = 50$) obtained with the original HardImageNet spurious ranking (Moayeri et al., 2022). Additionally, we compare it against a random baseline constructed as follows. For each (class, model), we take 16 random rankings, compute the PA Gap, and take the maximum; this procedure is then performed 16 times, we take the average as the baseline PA Gap for that (class, model) pair. Comparisons against these baselines provide evidence that we are capturing a statistically significant signal.

Next, we apply SpurLens to 79 COCO classes. (We exclude the "person“ class because (1) it is extremely generic and broad, making it outstandingly difficult to find strong spurious features for, and (2) it is several times larger than the second-largest class, making it very computationally expensive.) We use GPT-4 to generate 32 potential spurious features, and go through the same SpurLens process to compute PA Gaps with $K = 100$. Likewise, we compute random baselines for each class in the same manner.

(We emphasize that the Random Baseline is not a useful ranking method, but is provided as statistical evidence that the signal we measure cannot be explained as the result of random variations. The rankings produced by SpurLens are through object detection scores of spurious features and are thus interpretable, while the random rankings are not.)

Finally, we apply SpurLens to the 100 Imagenet classes from SpuriousImagenet (Neuhaus et al., 2023). PA Gaps are computed with $K = 50$, but otherwise the same procedure is used as for COCO.

Table 11: Comparison of class-wise averaged PA Gaps (as %) measured by SpurLens versus baselines. $K = 50$ for HardImageNet and Imagenet, and $K = 100$ for COCO.

Model	**HardImageNet**			**COCO**		**ImageNet Subset**	
	SpurLens Ranking	Original Ranking	Random Baseline	SpurLens Ranking	Random Baseline	SpurLens Ranking	Random Baseline
Qwen2-VL	5.9	5.8	5.3	15.2	8.7	6.7	5.0
Llama-3.2	15.0	12.1	8.5	14.8	8.6	17.7	9.4
LLaVA-v1.6	13.2	7.5	7.4	16.0	8.4	15.7	8.4
GPT-4o-mini	12.6	6.3	9.1	20.4	10.6	11.9	8.3

The class-wise averaged results of these experiments are presented in Table 11. We note that, while strong spurious features are not present in every class, SpurLens does tend to find significant spurious cues for most classes. The spurious gaps found by SpurLens for each class can be found in Appendix S.1 for HardImageNet, Appendix S.2 for COCO, and Appendix S.3 for the ImageNet subset. These results provide evidence that our methodology is both statistically significant and more effective than past work.

O Alternative Object Detectors

In the SpurLens pipeline, we use OWLv2 (Minderer et al., 2024) for open-set object detection to identify spurious features in a given image dataset. The reliability of OWLv2 is established in Appendix F. Here, we investigate using other open-set object detectors: GroundingDINO (Liu et al., 2024b) and YOLO World (Cheng et al., 2024). (Note that closed-vocabulary object detectors, such as DETR and many popular R-CNN variants, are not applicable to our methodology as we need to identify arbitrary spurious features/objects.)

Empirically, we observe that different object detectors have have different confidence behaviors and characteristics. GroundingDINO object detection results tend to have many false positives (incorrect labeled bounding boxes with fairly high confidence). Some qualitative examples of this are provided in Figure 19. This introduces significant noise, which leads to ranking errors and thus errors in Spurious Gap computation, especially for relatively small datasets such as HardImageNet classes (~ 1000 images per class). In contrast,

YOLO World tends to be very conservative in its confidence score estimates, and often misses instances of spurious objects; OWLv2 lies in the middle of these extremes, with the best overall performance that we observe empirically.

Nevertheless, we do find some agreement between f_i-scores computed with these different object detection systems. Figure 20 provides examples of correlations between OWLv2-based f_i-scores and both GroundingDINO-based f_i-scores and YOLO World-based f_i-scores, for select (target object, spurious feature) pairs from HardImageNet. We observe that the correlations are generally strong but varied and class/cue dependent. Nevertheless, they provide us with confidence that our pipeline is sound, and that OWLv2 is a strong choice of object detector for SpurLens.

P Dataset Diversity Evaluation

In Section 4, SpurLens assumes that we have access to a "large dataset of images", and that the dataset is sufficiently diverse to support object detection for spurious feature identification. Here, we clarify these heuristics and outline a simple procedure to examine a dataset's adequacy for use with SpurLens.

A simple minimum requirement for a spurious feature to be "sufficiently represented" in a dataset is for there to be at least K instances where it is present, and at least K instances where it is not, where K is the number of high-spurious and low-spurious images used for the MLLM evaluation. When analyzing GPT4-suggested spurious features, likely some will be sufficiently represented in a dataset, and some will not; a user would likely want at least $\widetilde{N}$ of the features to be sufficiently represented, for some reasonable value of $\widetilde{N}$. We would then run SpurLens on these features, and take the feature with the highest Spurious Gap, which we hope is positive, indicating that we identified a spurious correlation.

Suppose a user has a large dataset, and would like to test its diversity and suitableness before running the MLLM evaluation (the most expensive part of SpurLens). The user could perform feature proposal with GPT-4 to obtain N potential spurious cues (adjusting the prompt and providing additional domain-specific information, as needed, in order to obtain high-quality features for the downstream application). The user would choose $\widetilde{N} \leq N$, the minimum number of sufficiently-represented spurious cues they would like to evaluate on (using their heuristics and domain-specific knowledge to estimate how many spurious cues would likely be needed before getting at least one positive result). The user would perform the object detection step with OWLv2 on all N potential spurious cues.

For a given threshold $\tau \in [0, 1]$, a simple criteria is to believe that potential spurious cues with f_i-scores $> \tau$ have the image, and cues with f_i-score $< \tau$ do not have the image. Given τ, a user can compute the maximum value of K for each spurious cue such that it is sufficiently represented in the dataset. Finally, the user can compute the maximum K such that at least $\widetilde{N}$ of the spurious cues are sufficiently represented; call denote value $K_{\tau,\widetilde{N}}$. The user perform this calculation for various values of τ, and choose $\tau^\star$ with the maximal $K_{\tau^\star,\widetilde{N}}$. At this stage, the user can decide if the dataset is sufficiently diverse: if $K_{\tau^\star,\widetilde{N}}$ is sufficiently large, then they may proceed with the MLLM evaluation; otherwise, they must obtain a new dataset. The chosen value of K determines the accuracy and precision of SpurLens' PA Gap estimates; the user must determine what value of K is sufficiently large, based on their domain understanding and downstream objective.

As a case study, we apply this method to HardImageNet. In Figure 21, for various values of $\widetilde{N}$, we plot the minimum value of $K_{\tau^\star,\widetilde{N}}$ over all 15 HardImageNet classes against a range of τ values. We observe that $K_{\tau^\star,\widetilde{N}}$ is fairly high (over 100 in all cases). Additionally, if place harse restrictions on object detection confidence (such as $\tau > 0.3$), we are still able to achieve large K values ($K > 50$). This gives us confidence that HardImageNet is sufficiently diverse, and can support spurious feature detection and evaluation according to the standard SpurLens pipeline.

Q Class-wise Plots

We provided plots for other models in Figure 22.

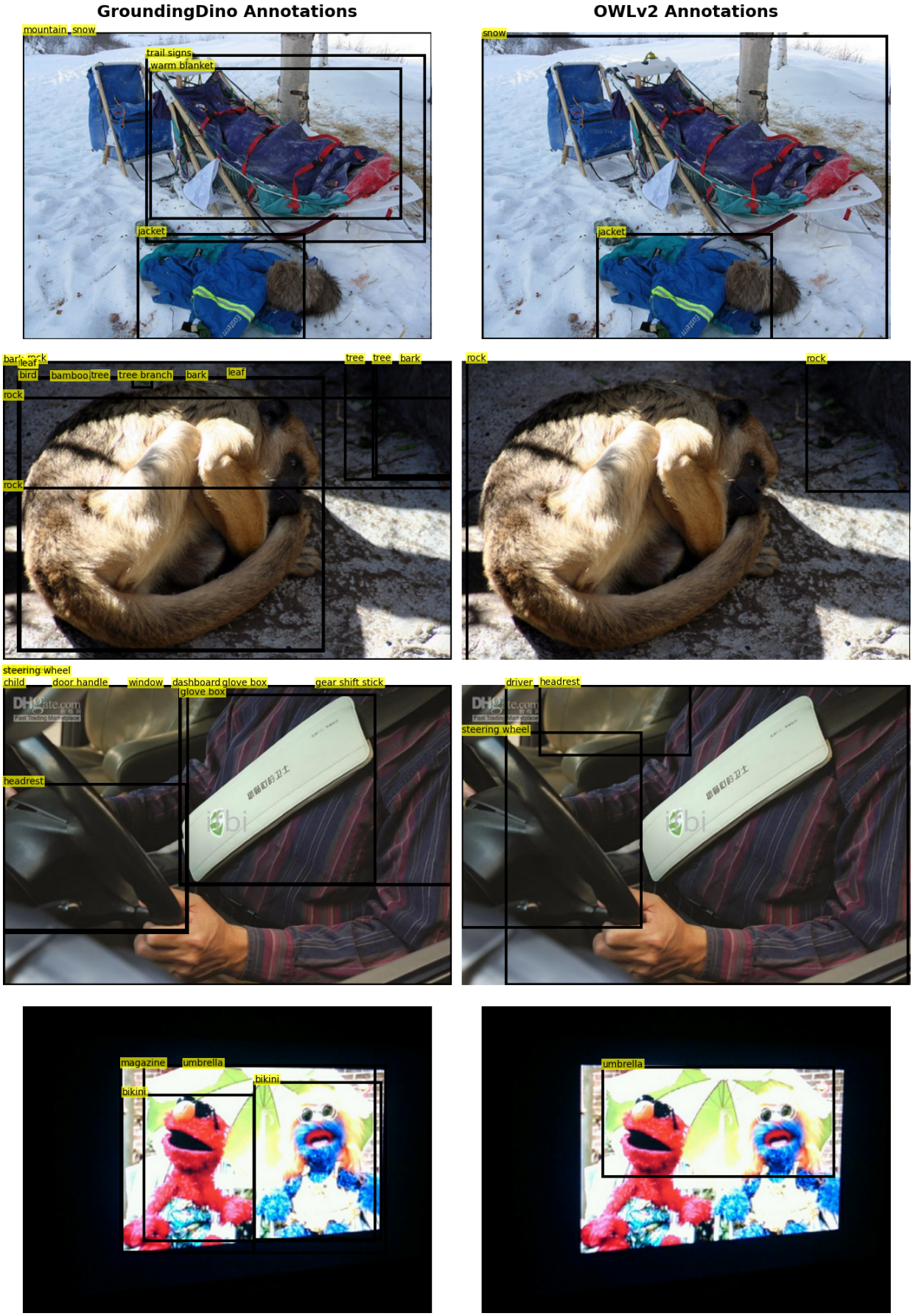

Figure 19: Qualitative examples comparing object detection with GroundingDino and OWLv2, taken from HardImageNet. OWLv2 is much more conservative with its bounding box proposals, while GroundingDino has many false positives before identifying the most pertinent queries features.

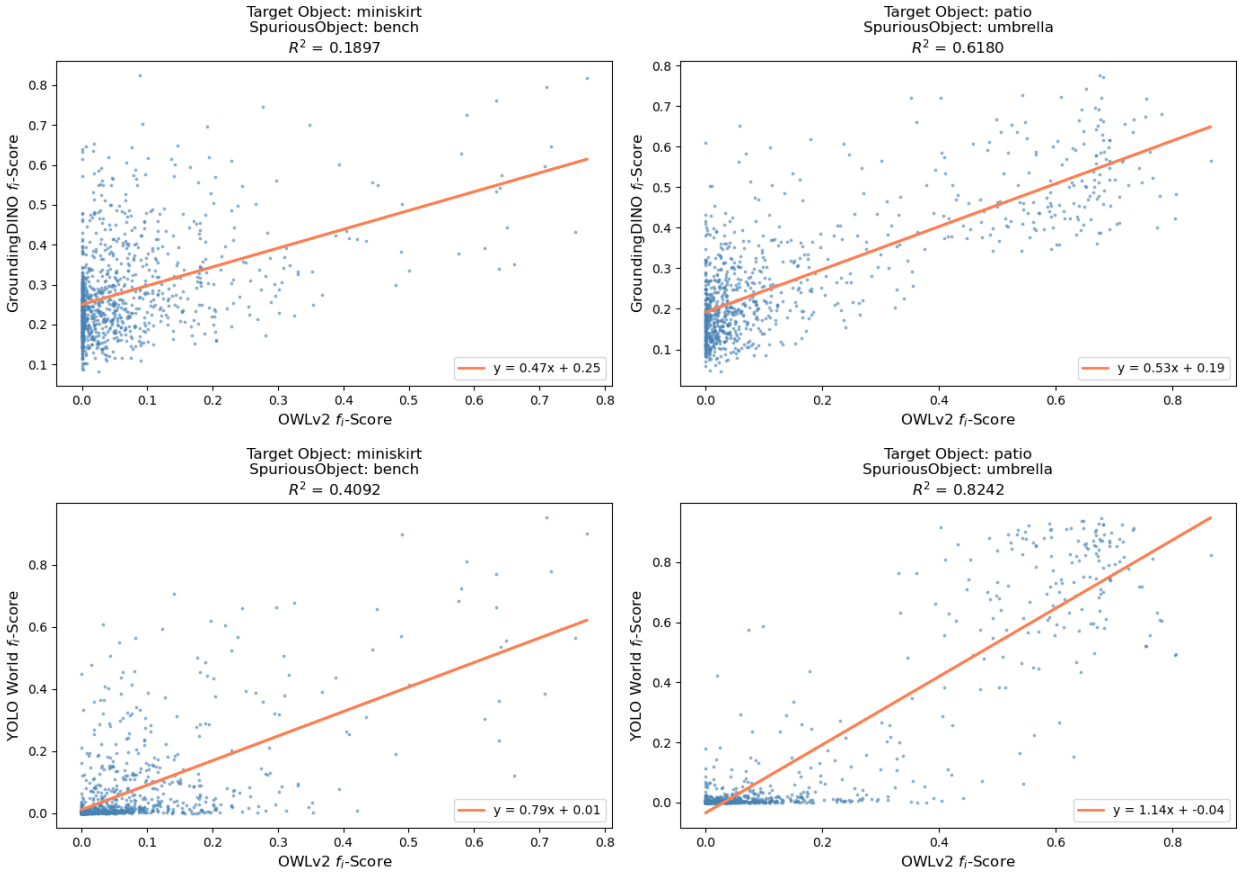

Figure 20: Plots comparing f_i-scores from OWLv2 to those from GroundingDINO and YOLO World object detection on two chosen (target object, spurious feature) pairs from HardImageNet. We observe that the correlation between the scores for the object detection models is object-dependent. We also observe the characteristics of these models: GroundingDINO tends to provide high detection scores to many images, while YOLO World is far far more conservative and gives near-0 scores to most images. OWLv2 lies between these extremes.

R Qualitative Examples of Spurious Gap

We highlighted some failures identified by *SpurLens* in Figure 23.

S Class-wise SpurLens Results

S.1 HardImageNet

As described in Section4, for each class, GPT-4 is used to generate 32 potential spurious features. We compute the PA Gap with $K = 50$ for these features, and choose feature with the maximum Gap. The results are in Table 12.

Additionally, we use token-dropping to turn each original image into an artificial negative example by dropping the tokens containing the target object. We compute the HR Gap with $K = 50$ for the same potential spurious features, and choose the feature with the maximum Gap. The results are in Table 13

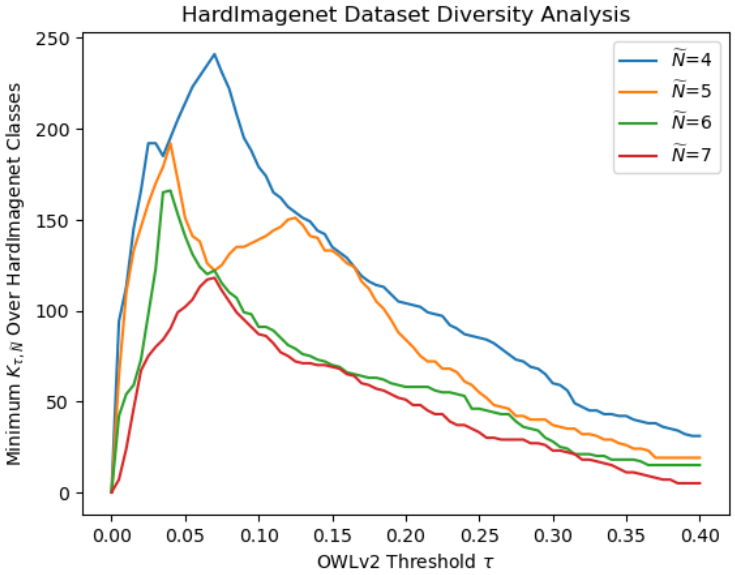

Figure 21: For various $\widetilde{N}$, we plot the minimum value of $K_{\tau,\widetilde{N}}$ over all 15 HardImageNet class for $\tau \in [0, 0.4]$. We observe that peak of each curve is above $K = 100$, supporting the fact that HardImageNet classes are diverse datasets and can support spurious object evaluation with (at least) $\widetilde{N} = 7$.

Table 12: Results of SpurLens applied to all 15 HardImageNet classes. For each model and for each class, we present the largest PA Gap (as %, with $K = 50$) and corresponding spurious feature found by SpurLens.

HardImageNet		**Qwen2-VL**		**Llama 3.2**		**LLaVa 1.6**		**GPT-4o-mini**	
Index	Name	Spur. Feat.	PA Gap	Spur. Feat.	PA Gap	Spur. Feat.	PA Gap	Spur. Feat.	PA Gap
0	dog sled	goggles	2.0	snow	22.0	snow	16.7	goggles	14.7
1	howler monkey	tree branch	2.0	tree branch	23.3	tree branch	6.7	tree branch	12.0
2	seat belt	rearview mirror	2.0	rearview mirror	6.7	headrest	8.0	driver	2.0
3	ski	helmet	2.0	chairlift	4.0	tree	4.0	goggles	6.0
4	sunglasses	water bottle	2.0	water bottle	5.3	camera	2.0	camera	6.0
5	swimming cap	floatation device	5.3	pool noodles	12.0	goggles	11.3	floatation device	8.0
6	balance beam	leotard	6.0	leotard	14.0	tumbling mats	15.3	playground	16.7
7	gymnastic horizontal bar	scoreboard	10.0	foam pit	17.3	foam pit	8.7	rope	10.7
8	patio	table	4.7	umbrella	9.3	rug	5.3	table	8.0
9	hockey puck	goalie stick	8.7	goalie stick	12.0	goalie stick	25.3	ice surface	9.3
10	miniskirt	grass	10.7	grass	28.7	bench	27.3	crop top	10.0
11	keyboard space bar	monitor stand	4.0	printer	29.3	monitor stand	14.0	screen	42.0
12	volleyball	sky	6.0	scoreboard	9.3	ankle braces	16.7	scoreboard	13.3
13	baseball player	spectator	6.7	batting gloves	18.0	spectator	20.0	spectator	8.7
14	snorkel	sand	16.7	sand	13.3	goggles	16.0	sand	22.0

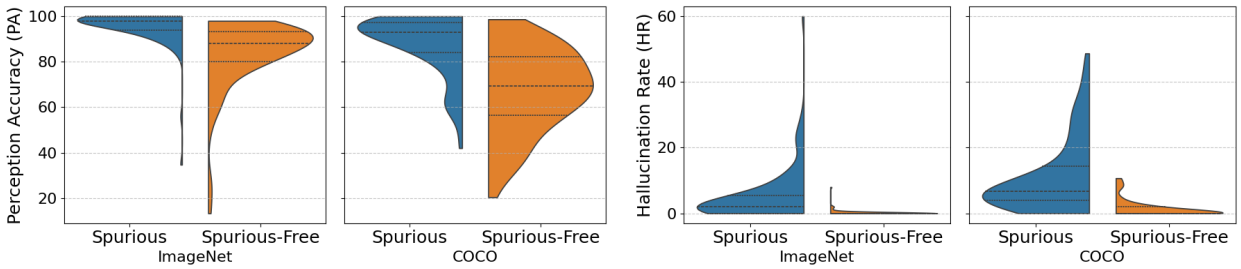

(a) GPT

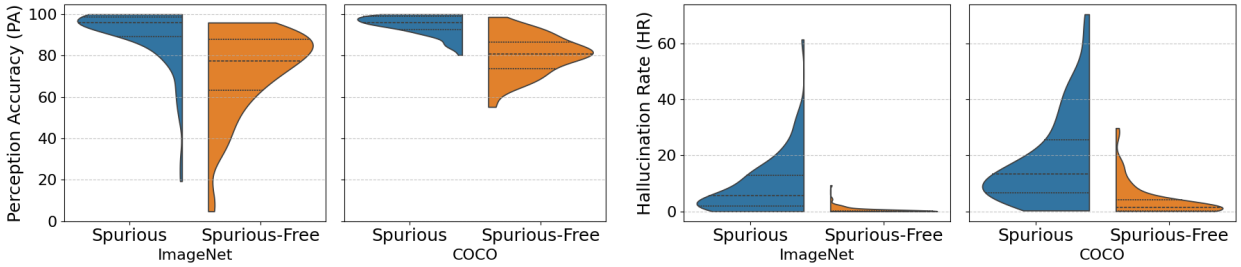

(b) Llama

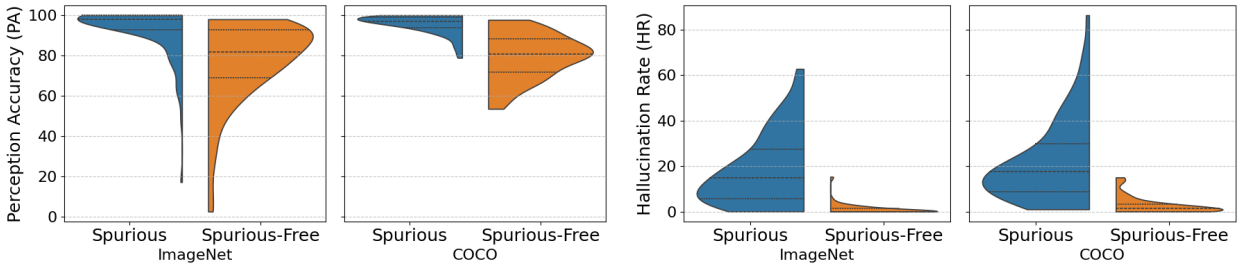

(c) LlaVA

Figure 22: Class-wise distribution of PA and HR for experiments in Section 5.1 and Section 5.2 respectively. These highlight the class-dependent nature of spurious biases.

Table 13: Results of SpurLens applied to all 15 HardImageNet classes with artificial negative examples through token-dropping. For each model and for each class, we present the largest HR Gap (as %, with $K = 50$) and corresponding spurious feature found by SpurLens.

HardImageNet		**Qwen2-VL**		**Llama 3.2**		**LLaVa 1.6**	
Index	Name	Spur. Feat.	HR Gap	Spur. Feat.	HR Gap	Spur. Feat.	HR Gap
0	dog sled	collar	38.0	collar	32.7	collar	44.7
1	howler monkey	fallen logs	8.7	banana	2.7	fallen leaves	9.3
2	seat belt	cup holder	12.7	headrest	27.3	headrest	38.0
3	ski	goggles	56.7	goggles	62.7	slope	66.0
4	sunglasses	cap	10.7	cap	17.3	cap	17.3
5	swimming cap	floatation device	23.3	floatation device	18.7	starting block	21.3
6	balance beam	tumbling mats	28.0	playground	38.0	tumbling mats	52.0
7	gymnastic horizontal bar	scoreboard	31.3	scoreboard	41.3	scoreboard	36.7
8	patio	table	28.0	cushion	30.0	table	18.7
9	hockey puck	goalie stick	18.0	goalie stick	18.0	goal net	16.7
10	miniskirt	sidewalk	41.3	handbag	8.0	sidewalk	36.7
11	keyboard space bar	cable	5.3	mouse pad	40.7	cable	11.3
12	volleyball	banner	37.3	referee stand	31.3	gymnasium	34.7
13	baseball player	umpire mask	51.3	umpire mask	38.0	umpire mask	50.0
14	snorkel	wet suit	15.3	wetsuit	20.7	flipper	36.9

Object: Bus, Spurious Cue: Curb

With Cue

Prompt: Determine whether there is a bus in the image.
Qwen2VL: Yes, there is a bus in the image.

Without Cue

Prompt: Determine whether there is a bus in the image.
Qwen2VL: No, there is no bus in the image.

Object: Tennis Racket, Spurious Cue: Court

With Cue

Prompt: Do you see a tennis racket in the image?
Qwen2VL: Yes, there is a tennis racket in the image.

Without Cue

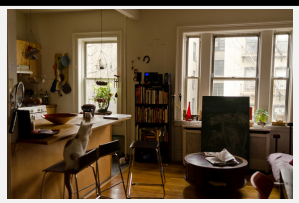

Prompt: Do you see a tennis racket in the image?
Qwen2VL: No, there is no tennis racket in the image.

Object: Hot Dog, Spurious Cue: Soda

With Cue

Prompt: Is there a hot dog in the image?
LLaVA-v1.6: Yes, there is a hot dog in the image. It is placed in a bun and topped with macaroni and cheese, and it appears to be covered in a sauce or condiment.

Without Cue

Prompt: Is there a hot dog in the image?
LLaVA-v1.6: No, there is no hot dog in the image. The image shows a variety of sandwiches and pastries displayed in a bakery or deli case.

Object: Cake, Spurious Cue: Candle

With Cue

Prompt: Is there a cake in the image?
Qwen2VL: Yes, there is a cake in the image.

Without Cue

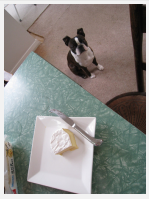

Prompt: Is there a cake in the image?
Qwen2VL: There is no existence of a cake in the image description.

Object: Vase, Spurious Cue: Flower

With Cue

Prompt: Determine whether there is a vase in the image.
Llama-3.2: Yes, there is a vase in the image. The vase is blue and contains orange flowers.

Without Cue

Prompt: Determine whether there is a vase in the image.
Llama-3.2: There are no vases in the image. The objects in the image appear to be candlesticks.

Figure 23: Visual examples from the COCO dataset. Object detection becomes more challenging for models when spurious cues are absent.

S.2 COCO

As described in Section 4, for 79 COCO classes, we use GPT-4 to generate 32 potential spurious features. We exclude COCO class 1 "person" from our analysis because (1) it is extremely generic and broad, making it outstandingly difficult to find good spurious features for, and (2) it is several times larger than the second-largest class, making it computationally expensive to analyze.

PA Gaps are computed with $K = 100$, and the feature with the largest Gap for each class is presented in Table 14.

To estimate HR Gaps, for each class, we take the images in the COCO superclass excluding the target class as the negative images dataset. For this experiment, we remove three additional classes ("sports ball", "dining table", and "keyboard") due to significant dataset error. We compute HR Gaps with the same spurious features and present the results in Table 15; we use $K = 50$ for GPT-4o-mini due to API costs, and $K = 100$ for all other models.

Finally, we also use token-dropping to turn images of each target object into artificial negative examples. HR Gaps and spurious features for these experiments are in Table 16.

Table 14: Results of SpurLens applied to almost all COCO classes. For each model and for each class, we present the largest PA Gap (as %, with $K = 100$) and corresponding spurious feature found by SpurLens.

COCO		**Qwen2-VL**		**Llama 3.2**		**LLaVa 1.6**		**GPT-4o-mini**	
Index	Name	Spur. Feat.	PA Gap	Spur. Feat.	PA Gap	Spur. Feat.	PA Gap	Spur. Feat.	PA Gap
2	bicycle	basket	16.5	basket	13.7	basket	10.0	water bottle	27.3
3	car	road	26.0	road	17.0	pavement markings	9.3	road	42.0
4	motorcycle	mirror	12.2	glove	13.3	glove	14.0	glove	22.3
5	airplane	control tower	3.0	turbine	7.9	turbine	5.0	turbine	8.4
6	bus	curb	18.0	signage	15.7	curb	18.7	curb	25.3
7	train	fence	1.7	fence	4.3	fence	4.0	fence	6.7
8	truck	hitch	43.3	roof rack	23.5	hitch	33.9	hitch	52.4
9	boat	oar	19.5	buoy	12.7	dock	18.7	fishing gear	27.0
10	traffic light	street sign	21.0	street sign	24.3	street sign	21.0	street sign	35.3
11	fire hydrant	storm drain	14.3	storm drain	12.7	storm drain	18.0	storm drain	21.3
13	stop sign	tree	10.0	tree	14.3	landscape	12.7	tree	18.0
14	parking meter	ticket	31.0	ticket	23.7	ticket	20.3	ticket	28.7
15	bench	bush	18.7	flowerbed	16.0	book	19.4	tree	25.3
16	bird	leaf	17.3	branch	16.7	branch	23.7	branch	18.7
17	cat	collar	4.0	collar	5.0	scratching post	4.1	collar	5.7
18	dog	collar	21.8	collar	30.2	collar	14.3	collar	28.1
19	horse	saddle	9.7	saddle	7.7	saddle	10.0	saddle	10.3
20	sheep	path	3.0	pasture	15.0	pasture	9.0	pasture	12.0
21	cow	farmer	9.1	barn	13.2	barn	13.3	barn	11.5
22	elephant	mud	5.0	mud	7.3	mud	9.3	mud	6.3
23	bear	rock	3.7	grass	7.7	grass	3.3	grass	5.0
24	zebra	trail	1.0	dirt	1.3	grass	3.0	dirt	3.0
25	giraffe	fence	0.7	barbwire	2.0	savannah	2.3	savannah	1.3
27	backpack	pen	16.7	laptop	16.0	key	19.7	pen	24.3
28	umbrella	raincoat	10.0	bag	10.7	bag	9.0	raincoat	22.7
31	handbag	bag stand	20.0	lipstick	17.2	key	21.0	wallet	39.8
32	tie	lapel pin	33.3	suit	35.3	lapel pin	17.7	pocket square	30.7
33	suitcase	baggage cart	36.5	baggage cart	15.7	travel brochure	17.3	baggage cart	28.3
34	frisbee	park	4.0	tree	7.0	park	8.3	tree	4.7
35	skis	pole	7.7	glove	14.3	snowboard	13.4	glove	14.3
36	snowboard	pant	19.2	pant	18.4	terrain park	23.0	pant	23.8
37	sports ball	turf	11.3	jersey	10.7	referee	10.3	referee	15.0
38	kite	child	2.0	fence	5.7	field	3.0	fence	7.7
39	baseball bat	uniform	5.5	uniform	8.8	uniform	27.1	uniform	8.2
40	baseball glove	cap	12.0	cleat	27.7	cleat	21.0	grass	22.3
41	skateboard	wall	2.0	shoe	5.0	shoe	4.0	shoe	4.3
42	surfboard	bikini	5.7	wave	6.7	bikini	5.7	bikini	8.3
43	tennis racket	court	12.0	court	18.0	court	19.3	court	14.3
44	bottle	ice	13.4	cup	8.7	ice	12.8	table	24.0
46	wine glass	candle	13.3	cutlery	11.7	cutlery	12.7	cheese	18.5
47	cup	spoon	24.3	table	18.7	coaster	24.7	biscuit	32.0
48	fork	sauce	20.7	sauce	20.3	plate	14.0	plate	21.0
49	knife	chopping block	21.0	cutlery holder	15.0	chopping block	14.7	chopping block	40.0
50	spoon	bowl	28.5	food	35.4	sugar	25.3	sugar	20.8
51	bowl	granola	27.3	granola	15.3	granola	19.7	fruit	34.7
52	banana	coconut	4.7	fruit label	9.6	coconut	9.0	coconut	12.0
53	apple	table	7.7	knife	5.3	table	10.7	tree	15.3
54	sandwich	mayonnaise	18.9	pickle	21.0	pickle	18.8	mayonnaise	23.8

Continued on the next page

COCO		Qwen2-VL		Llama 3.2		LLaVa 1.6		GPT-4o-mini	
Index	Name	Spur. Feat.	PA Gap	Spur. Feat.	PA Gap	Spur. Feat.	PA Gap	Spur. Feat.	PA Gap
55	orange	fruit basket	15.3	fruit basket	10.7	fruit basket	14.7	fruit basket	14.5
56	broccoli	chicken	14.0	chicken	13.0	chicken	11.3	quinoa	18.8
57	carrot	vegetable	30.5	vegetable	29.0	vegetable	33.6	vegetable	31.5
58	hot dog	ketchup	12.2	ketchup	17.7	ketchup	24.4	ketchup	23.7
59	pizza	olive	8.8	onion	10.1	olive	14.0	mushroom	12.0
60	donut	box	7.7	box	6.7	box	3.7	box	13.7
61	cake	candle	24.0	candle	23.3	candle	24.0	candle	31.0
62	chair	cushion	26.3	lamp	14.0	table	29.3	table	32.3
63	couch	throw pillows	14.7	throw pillows	14.5	throw pillows	36.4	throw pillows	20.1
64	potted plant	tag	14.8	floor	15.7	vase	12.6	curtain	21.7
65	bed	sheet	23.1	sheet	21.9	sheet	29.4	sheet	34.7
67	dining table	napkin	23.0	plate	34.7	centerpiece	21.7	chair	53.0
70	toilet	sanitary bin	10.0	shower curtain	9.3	sanitary bin	16.3	sanitary bin	12.0
72	tv	dvd player	39.7	coffee table	31.7	sound system	40.0	dvd player	42.7
73	laptop	mouse	10.3	mouse	11.3	headphone	9.7	mouse	15.3
74	mouse	paper	4.3	computer	11.0	computer	12.7	computer	13.3
75	remote	blanket	8.0	carpet	6.3	couch	2.3	blanket	1.3
76	keyboard	wrist rest	42.2	wrist rest	19.1	wrist rest	45.7	wrist rest	67.2
77	cell phone	sunglass	9.3	watch	9.7	sunglass	10.0	sunglass	7.7
78	microwave	coffee maker	8.7	cabinet	12.7	oven	23.3	countertop	9.7
79	oven	cooling rack	23.3	wall	17.7	pan	21.0	microwave	22.0
80	toaster	cutting board	9.7	kitchen counter	10.7	microwave	12.3	kitchen counter	9.3
81	sink	sponge holder	18.4	towel	11.3	sponge holder	13.4	sponge holder	23.6
82	refrigerator	magnet	18.7	magnet	20.0	magnet	37.7	magnet	19.3
84	book	blanket	14.7	coaster	10.7	lamp	16.7	clock	13.3
85	clock	wall	23.7	sign	17.3	wall	17.7	wall	25.0
86	vase	leaf	27.3	flower	30.0	leaf	19.7	leaf	33.0
87	scissors	marker	9.3	felt	20.6	glue	11.2	felt	10.3
88	teddy bear	cuddly blanket	6.0	crib	3.0	cuddly blanket	3.0	cuddly blanket	9.0
89	hair drier	conditioner	6.0	conditioner	12.0	conditioner	5.0	basket	10.7
90	toothbrush	comb	10.1	floss	9.3	comb	12.0	comb	6.0

Table 15: For almost all COCO classes, we apply SpurLens to other images in the same superclass. For each model and class, we present the largest HR Gap (as %), and corresponding spurious features. We use $K = 50$ for GPT-4o-mini and $K = 100$ for the other models.

COCO		Qwen2-VL		Llama 3.2		LLaVa 1.6		GPT-4o-mini	
Index	Name	Spur. Feat.	HR Gap	Spur. Feat.	HR Gap	Spur. Feat.	HR Gap	Spur. Feat.	HR Gap
2	bicycle	basket	24.0	lamp post	11.3	basket	24.3	sidewalk	8.0
3	car	tree	17.3	traffic signs	17.7	tree	17.3	tree	17.3
4	motorcycle	mirror	10.0	billboard	9.8	billboard	6.7	barrier	1.3
5	airplane	baggage cart	1.3	sky	2.7	luggage	1.3	car	0.7
6	bus	traffic light	1.7	traffic cone	12.7	post box	6.3	tree	3.3
7	train	graffiti	2.3	bridge	3.3	bridge	12.3	bridge	4.0
8	truck	hitch	8.3	roof rack	22.5	parking lot	24.0	sign	9.3
9	boat	sail	15.0	dock	28.8	dock	25.0	dock	18.7
10	traffic light	bus stop	7.7	crosswalk	10.7	bus stop	7.7	crosswalk	8.7
11	fire hydrant	car	9.0	street	10.2	storm drain	18.7	storm drain	9.3
13	stop sign	crosswalk	9.7	side street	7.0	utility pole	15.3	side street	4.7
14	parking meter	car	2.3	bus stop	8.7	bus stop	18.0	curb	5.3
15	bench	trashcan	5.0	umbrella	12.7	coffee cup	6.0	coffee cup	8.0
16	bird	pond	3.0	sky	7.8	feeder	18.3	bush	4.0
17	cat	tv	5.3	furniture	5.2	shelf	8.3	door	5.3
18	dog	collar	3.7	bed	7.5	toy	8.0	bed	8.7
19	horse	saddle	6.0	barn	4.0	saddle	19.3	trailer	6.0
20	sheep	hill	6.0	hill	4.7	shepherd	6.3	hill	5.3
21	cow	farmer	6.7	road	7.0	road	17.3	hill	7.3
22	elephant	sky	0.7	bamboo	0.7	path	1.0	mud	0.0
23	bear	rock	0.0	cave	0.0	river	1.3	log	0.0
24	zebra	bush	1.0	antelope	2.0	antelope	1.0	bird	0.0
25	giraffe	safari vehicle	1.0	cloud	0.5	horizon	2.0	safari vehicle	1.3
27	backpack	charger	23.0	laptop	20.3	first aid kit	26.7	trail	16.0
28	umbrella	raincoat	9.3	raincoat	6.2	flower pot	6.0	dog	2.0
31	handbag	notebook	43.3	notebook	25.2	notebook	35.0	sofa	10.7
32	tie	suit	14.7	suit	10.0	suit	40.3	suit	15.3
33	suitcase	baggage cart	7.3	concrete floor	13.8	travel pillow	22.7	baggage cart	6.7
34	frisbee	dog	5.3	dog	5.8	dog	18.7	people	2.0
35	skis	snow shovel	10.7	snow shovel	13.3	snow pants	65.0	snow shovel	12.0
36	snowboard	goggle	6.7	snow	4.2	goggles	17.7	terrain park	4.0
38	kite	field	3.3	horizon	2.7	horizon	7.0	horizon	4.7
39	baseball bat	home plate	9.0	ballpark	14.8	home plate	6.0	ballpark	6.0
40	baseball glove	uniform	15.3	uniform	16.0	bat	21.0	uniform	9.3
41	skateboard	sticker	7.7	ramp	4.0	ramp	13.3	street	4.0

Continued on the next page

COCO		Qwen2-VL		Llama 3.2		LLaVa 1.6		GPT-4o-mini	
Index	Name	Spur. Feat.	HR Gap	Spur. Feat.	HR Gap	Spur. Feat.	HR Gap	Spur. Feat.	HR Gap
42	surfboard	paddle	8.0	wetsuit	9.2	wetsuit	16.7	fishing boat	4.7
43	tennis racket	court	2.0	court	2.0	court	3.0	court	4.0
44	bottle	counter	6.0	wall	28.7	box	8.3	cup	22.7
46	wine glass	candle	6.3	cork	12.5	coaster	19.0	cork	5.3
47	cup	tea	35.3	tea	33.7	tea	25.0	tea	22.7
48	fork	plate	8.0	food	28.5	food	45.3	cheese	20.0
49	knife	cutlery holder	21.3	utensil	32.0	utensil	40.0	utensil	12.0
50	spoon	whisk	20.0	chopstick	30.2	whisk	36.0	whisk	21.3
51	bowl	pudding	17.3	pudding	27.7	vegetable	26.3	ice cream	26.0
52	banana	coconut	17.3	paper towel	5.7	coconut	6.3	wall	10.0
53	apple	basket of fruit	6.7	picnic blanket	6.7	basket of fruit	12.3	table	2.0
54	sandwich	mustard	31.3	mustard	67.7	mustard	66.7	mustard	40.7
55	orange	wall	11.3	wall	4.7	wall	20.7	cutting board	9.0
56	broccoli	lemon	7.3	lemon	8.0	carrot	11.7	napkin	4.0
57	carrot	vegetable	15.7	soup	11.2	vegetable	37.0	bowl	3.3
58	hot dog	soda	2.3	cheese	2.8	relish	2.0	cheese	6.7
59	pizza	basil	2.7	olive	4.3	knife	2.0	basil	2.0
60	donut	coffee	6.0	coffee	2.2	coffee	5.7	table	2.0
61	cake	chocolate	9.0	chocolate	12.7	candle	12.0	candle	4.0
62	chair	cushion	35.7	footrest	44.7	footrest	52.3	cushion	46.7
63	couch	blanket	27.3	television	17.3	coffee table	14.3	coffee table	21.3
64	potted plant	vase	51.7	vase	24.3	vase	83.0	vase	36.7
65	bed	sheet	19.0	sheet	21.7	sheet	13.0	nightstand	14.7
70	toilet	diaper pail	3.3	sink	9.8	sink	2.3	sink	8.7
72	tv	game console	4.7	couch	27.7	coffee table	11.7	rug	4.0
73	laptop	mouse	13.3	webcam	13.3	chair	13.0	mouse	10.0
74	mouse	computer	9.3	computer	13.0	paper	10.0	lab equipment	0.7
75	remote	floor	9.3	coaster	28.7	window	22.7	blanket	4.0
77	cell phone	charger	7.7	key	10.0	bag	11.7	book	8.7
78	microwave	cooking tray	4.0	oven	22.7	oven	9.3	plastic wrap	6.7
79	oven	pan	19.7	microwave	44.5	pan	21.7	microwave	28.7
80	toaster	knife	23.7	coffee maker	19.7	microwave	50.3	knife	20.0
81	sink	trash can	8.7	trash can	11.0	knife	23.0	trash can	18.0
82	refrigerator	magnet	13.7	magnet	14.3	magnet	14.3	magnet	25.3
84	book	lamp	9.3	note	24.3	pencil	12.7	pencil	4.7
85	clock	lamp	10.0	alarm button	9.0	alarm button	7.3	alarm button	6.7
86	vase	flower	18.0	flower	38.8	plant	30.3	flower	17.3
87	scissors	marker	28.3	cardboard	6.7	glue	35.0	glue	2.0
88	teddy bear	cuddly blanket	13.0	bed	6.5	cuddly blanket	14.3	book	4.0
89	hair drier	conditioner	10.0	conditioner	5.8	shampoo	40.7	makeup remover	4.0
90	toothbrush	toothpaste	11.3	comb	13.8	comb	24.0	shaving cream	4.0

Table 16: Results of SpurLens applied to almost all COCO classes with token-dropping to artificially create negative samples. For each model and for each class, we present the largest HR Gap (as %, with $K = 100$) and corresponding spurious feature found by SpurLens.

COCO		Qwen2-VL		Llama 3.2		LLaVa 1.6	
Index	Name	Spur. Feat.	HR Gap	Spur. Feat.	HR Gap	Spur. Feat.	HR Gap
2	bicycle	helmet	22.0	helmet	16.3	helmet	32.7
3	car	billboard	16.7	mountain	15.6	billboard	8.7
4	motorcycle	helmet	66.7	helmet	21.8	helmet	61.3
5	airplane	turbine	19.6	sky	13.9	turbine	22.3
6	bus	parking meter	5.9	crosswalk	11.8	signage	7.0
7	train	graffiti	10.1	graffiti	11.1	tunnel	8.0
8	truck	hitch	12.6	roof rack	16.2	parking lot	36.5
9	boat	fishing gear	26.7	buoy	21.2	buoy	34.4
10	traffic light	pedestrian	18.3	crosswalk	21.1	curb	23.3
11	fire hydrant	sidewalk	12.0	street	12.2	storm drain	11.3
13	stop sign	side street	18.6	side street	7.8	traffic light	10.3
14	parking meter	pavement	14.5	curb	10.9	bus stop	20.7
15	bench	sunglass	25.0	laptop	23.6	book	28.1
16	bird	branch	12.7	mountain	17.9	water	12.0
17	cat	scratching post	14.3	scratching post	5.7	scratching post	14.0
18	dog	leash	7.0	leash	4.5	leash	12.7
19	horse	riding boots	38.3	jumping poles	11.1	stirrup	14.7
20	sheep	barn	11.3	barn	9.4	hill	10.7

Continued on the next page

COCO		Qwen2-VL		Llama 3.2		LLaVa 1.6	
Index	Name	Spur. Feat.	HR Gap	Spur. Feat.	HR Gap	Spur. Feat.	HR Gap
21	cow	animal pen	10.3	pasture gate	12.1	bale	13.9
22	elephant	sand	5.3	bush	0.0	waterhole	7.0
23	bear	tree	5.0	river	4.6	tree	2.3
24	zebra	waterhole	12.0	waterhole	16.8	waterhole	5.3
25	giraffe	waterhole	7.0	savannah	6.0	waterhole	5.3
27	backpack	first aid kit	26.6	water bottle	12.6	first aid kit	24.0
28	umbrella	lamp post	8.7	bag	18.6	people	27.1
31	handbag	bag stand	32.9	key	16.2	bag stand	27.5
32	tie	suit	22.7	pocket square	14.0	suit	56.3
33	suitcase	baggage cart	38.3	baggage cart	32.0	waiting area	43.0
34	frisbee	people	28.2	bicycle	14.0	tree	28.0
35	skis	glove	43.0	glove	55.2	snow pants	42.6
36	snowboard	glove	51.0	glove	52.0	terrain park	31.7
37	sports ball	jersey	11.0	jersey	38.4	referee	21.3
38	kite	backpack	18.0	mountain	16.7	camera	7.3
39	baseball bat	helmet	55.3	umpire's gear	59.6	helmet	22.3
40	baseball glove	bat	17.7	uniform	29.5	bat	41.3
41	skateboard	ramp	50.0	ramp	29.1	ramp	27.7
42	surfboard	wetsuit	36.0	wave	32.1	wetsuit	30.0
43	tennis racket	line	16.7	line	21.1	line	20.0
44	bottle	wall	9.9	cabinet	30.6	box	13.3
46	wine glass	candle	14.0	ice bucket	16.5	ice bucket	18.0
47	cup	window	8.3	tea	23.8	tea	23.7
48	fork	chair	16.0	chair	18.0	chair	33.0
49	knife	chef hat	13.4	cutlery holder	30.0	pan	20.0
50	spoon	whisk	21.3	food	26.8	chopstick	26.3
51	bowl	rice	14.3	yogurt	22.8	dishcloth	26.7
52	banana	coconut	41.3	coconut	21.8	coconut	40.7
53	apple	crate	26.6	crate	14.6	crate	34.7
54	sandwich	basket	6.3	chip	19.6	cheese	5.9
55	orange	wooden crate	38.2	wooden crate	14.8	wooden crate	43.0
56	broccoli	pan	17.7	pasta	20.9	quinoa	18.4
57	carrot	vegetable	26.5	fruit	0.0	vegetable	55.5
58	hot dog	grill	16.7	soda	10.2	grill	8.3
59	pizza	parchment paper	22.2	light fixture	10.6	light fixture	16.7
60	donut	display stand	37.7	display stand	26.5	display stand	33.0
61	cake	banner	22.3	balloon	17.6	banner	18.3
62	chair	footrest	20.7	footrest	16.3	footrest	38.6
63	couch	pillow	13.8	coffee cup	18.6	throw pillows	18.1
64	potted plant	tag	16.9	tag	20.1	pebble	21.0
65	bed	throw blanket	18.4	book	17.0	teddy bear	16.9
67	dining table	napkin	30.8	chair	26.9	silverware	33.4
70	toilet	sanitary bin	13.7	wall art	18.6	sanitary bin	13.0
72	tv	sound system	16.6	dvd player	41.6	dvd player	42.7
73	laptop	desk	15.3	desk	21.3	sticky notes	13.7
74	mouse	lab equipment	5.3	computer	10.7	lab equipment	16.3
75	remote	charger	32.3	wall	28.0	speaker	25.3
76	keyboard	wrist rest	11.9	chair	21.7	sticky notes	11.3
77	cell phone	sunglass	17.7	sunglass	28.9	sunglass	21.0
78	microwave	trash bin	9.7	fruit bowl	24.9	oven	11.7
79	oven	apron	31.7	baking sheet	12.8	pan	20.9
80	toaster	cutting board	8.0	wall cabinets	9.7	microwave	28.0
81	sink	sponge holder	24.4	towel	30.4	sponge	26.7
82	refrigerator	milk	11.9	milk	17.7	yogurt	7.8
84	book	pencil	7.7	clock	17.1	note	9.2
85	clock	lamp	13.7	table	3.1	chair	2.3

Continued on the next page

COCO		Qwen2-VL		Llama 3.2		LLaVa 1.6	
Index	Name	Spur. Feat.	HR Gap	Spur. Feat.	HR Gap	Spur. Feat.	HR Gap
86	vase	decorative balls	15.6	flower	51.6	flower	40.7
87	scissors	marker	16.7	craft box	8.7	craft box	47.1
88	teddy bear	toy box	20.3	toy box	16.3	toy box	32.0
89	hair drier	toothbrush	10.7	brush	13.7	shampoo	34.7
90	toothbrush	comb	14.3	toothpaste	22.6	toothpaste	44.7

S.3 Imagenet Subset

As described in Section 4, the 100 Imagenet classes considered in Spurious Imagenet (Neuhaus et al., 2023), we use GPT-4 to generate 32 potential spurious features.

PA Gaps are computed with $K = 50$, and the feature with the largest Gap for each class is presented in Table 17.

To estimate HR Gaps, for each class, we randomly sample 5000 images from the other 99 classes. We compute HR Gaps (with $K = 50$) with the same spurious features, and present the results in Table 18.

Table 17: Results of SpurLens applied to 100 Imagenet classes. For each model and for each class, we present the largest PA Gap (as %, with $K = 50$) and corresponding spurious feature found by SpurLens.

Imagenet		Qwen2-VL		Llama 3.2		LLaVa 1.6		GPT-4o-mini	
Index	Name	Spur. Feat.	PA Gap	Spur. Feat.	PA Gap	Spur. Feat.	PA Gap	Spur. Feat.	PA Gap
0	tench	net	10.0	reed	22.0	fishing rod	18.0	reed	5.3
2	great white shark	boat	7.3	fish	18.7	fish	20.7	fish	14.0
14	indigo bunting	branch	0.0	branch	6.7	stone	2.0	branch	4.7
42	agama	rock	2.7	rock	19.3	rock pile	18.7	stone	9.3
50	American alligator	turtle	4.0	lily pads	24.7	water	21.3	water	17.3
58	water snake	cattail	3.3	dragonfly	6.7	pond	30.7	reed	6.0
80	black grouse	grass	16.0	grass	18.0	grass	14.7	grass	14.7
81	ptarmigan	sky	2.0	boulder	4.0	mountain	25.3	sky	2.0
82	ruffed grouse	bush	12.0	branch	34.7	grass	14.0	branch	26.7
89	sulphur-crested cockatoo	feeder	0.0	tree	29.3	feeder	8.0	bush	4.0
91	coucal	nest	10.0	bark	18.0	tree	28.7	nest	12.0
94	hummingbird	sky	2.0	sky	4.0	feeder	6.7	sky	2.0
103	platypus	bubble	4.7	bubble	23.3	branch	18.0	bubble	9.3
105	koala	eucalyptus leaves	1.3	foliage	6.0	foliage	2.0	eucalyptus leaves	4.0
147	grey whale	dolphin	4.0	fisherman	36.0	dolphin	29.3	beach	16.7
288	leopard	fence	0.0	tree	16.0	waterhole	8.0	tree	18.7
297	sloth bear	rock	4.0	waterhole	20.0	tree	14.7	rock	12.7
309	bee	grass	0.0	garden	6.0	garden	0.0	garden	0.7
313	stick insect	stone	1.3	water droplet	-1.3	dirt mound	1.3	dirt mound	3.3
324	small white butterfly	grass	3.3	garden	19.3	garden	14.7	wildflower	3.3
325	sulphur butterfly	stone	6.0	twig	6.7	bee	8.0	grass	5.3
335	fox squirrel	tree	16.0	tree	30.0	tree	22.7	tree	16.0
351	hartebeest	muddy ground	0.0	rock	15.3	waterhole	18.7	horizon	5.3
364	three-toed sloth	bird	2.0	rock	13.3	tree	12.0	bird	2.0
379	howler monkey	branch	4.0	branch	37.3	branch	5.3	branch	10.7
384	indri	tree	12.0	tree	20.0	branch	21.3	tree	60.7
389	snoek fish	bait	7.3	cooler	14.7	bait	24.0	tide pool	21.3
394	sturgeon	camera	1.7	glove	5.3	riverbed	20.7	net	5.3
395	gar fish	bait	12.0	bait	27.3	bait	13.3	turtle	29.3
400	academic gown	desk	2.0	diploma	5.3	diploma	4.0	flower	6.0
415	bakery	signpost	24.0	car	38.7	signpost	28.0	signpost	36.0
416	balance beam	camera	6.0	camera	14.0	rope	24.7	camera	17.3
419	Band-Aid	alcohol wipes	0.7	alcohol wipes	18.0	skin	12.0	skin	12.7
424	barbershop	pavement	2.0	pavement	18.0	tree	8.0	flowerpot	4.0
425	barn	bucket	2.0	haystack	6.0	windmill	6.0	windmill	9.3
433	swimming cap	bleacher	4.7	paddle	13.3	lifeguard	17.3	water bottle	8.0
434	bath towel	sink	2.7	mirror	33.3	shelf	2.0	showerhead	5.3
435	bathtub	brush	4.0	brush	14.0	soap	48.0	wall tiles	10.0
440	beer bottle	chip	2.0	table	12.0	chair	6.0	table	5.3
445	bikini	cooler	5.3	beach umbrella	10.7	cooler	4.7	cooler	8.7
454	bookstore	picture frame	5.3	picture frame	14.0	laptop	3.3	laptop	7.3
465	bulletproof vest	picture	0.0	tactical belt	33.3	tactical belt	23.3	tactical belt	7.3
466	high-speed train	overpass	9.3	overpass	14.0	overpass	22.7	overpass	12.0
490	chain mail	tent	4.7	stone wall	14.0	sword stand	7.3	forest	15.3
491	chainsaw	work boots	4.0	work boots	8.7	trailer	5.3	work boots	9.3
515	cowboy hat	saddle	3.3	guitar	10.7	plain	4.0	fence	8.0
516	cradle	changing table	6.0	nursery rug	24.0	nursery rug	11.3	photo frame	7.3
525	dam	bridge	13.3	bridge	36.0	bridge	14.0	bridge	14.7

Continued on the next page

Imagenet		Qwen2-VL		Llama 3.2		LLaVa 1.6		GPT-4o-mini	
Index	Name	Spur. Feat.	PA Gap	Spur. Feat.	PA Gap	Spur. Feat.	PA Gap	Spur. Feat.	PA Gap
537	dog sled	ski tracks	2.7	ski tracks	28.0	ski tracks	21.3	ski tracks	23.3
543	dumbbell	kettlebell	6.0	fitness tracker	12.7	floor tiles	8.0	yoga block	6.0
554	fireboat	tugboat	24.7	coast guard	29.3	tugboat	46.0	tugboat	35.7
557	flagpole	cloud	4.0	bench	6.0	cloud	8.0	sign	6.7
563	fountain pen	stapler	2.0	ink bottle	8.0	ink bottle	8.7	stamp	10.0
565	freight car	crane	0.7	warehouse	7.3	crane	4.0	warehouse	3.3
576	gondola	flag	2.0	canal	12.7	paddle	5.3	canal	7.3
585	hair spray	bobby pins	14.3	bobby pins	38.0	bobby pins	16.7	conditioner	18.7
588	hamper	wall	24.7	cup	27.3	curtain	16.0	image	10.7
592	hard disk drive	desk	-1.3	keyboard	4.0	printer	4.7	wall	-2.7
602	gymnastic horizontal bar	exercise balls	8.7	ring	9.3	jump rope	7.3	ring	7.3
626	lighter	cell phone	0.7	cell phone	7.3	keychain	16.7	matchstick	6.7
655	miniskirt	jacket	6.7	belt	14.0	streetlamp	32.7	grass	4.0
667	graduation cap	flag	4.0	diploma	5.3	gown	4.7	diploma	4.0
671	mountain bike	backpack	4.7	rock	12.7	bush	8.0	backpack	15.3
678	neck brace	lamp	11.3	wall	26.7	magazine	8.0	lamp	6.0
680	baby pacifier	teething toy	72.0	teething toy	75.3	teething toy	40.0	teething toy	72.7
682	obelisk	sidewalk	2.0	mountain	4.0	sidewalk	2.0	cloud	3.3
684	ocarina	headphone	2.7	photo	-1.3	table	0.0	headphone	5.3
695	padlock	bag	2.0	post	6.0	box	4.7	gate	2.0
702	parallel bars	pull-up bar	9.3	wrist tape	15.3	pull-up bar	20.0	pull-up bar	10.7
709	pencil case	clip	12.0	clip	36.0	clip	58.7	clip	8.7
720	pill bottle	first aid kit	4.7	inhaler	19.3	glass of water	11.3	inhaler	6.7
722	ping-pong ball	referee	7.3	racket	25.3	racket	36.0	floor	8.0
728	plastic bag	tissue	2.0	water bottle	8.7	tissue	3.3	tissue	2.7
731	plunger	soap	12.7	faucet	22.0	tile	42.0	trashcan	12.7
733	pole	road	3.3	cloud	12.0	cloud	9.3	cloud	8.0
737	soda bottle	table	2.7	chair	20.0	chair	14.0	straw	4.7
738	plant pot	vase	16.7	vase	15.3	vase	19.3	vase	12.0
739	potter's wheel	display	2.7	brush	21.3	clay	12.6	water	13.3
746	hockey puck	helmet	9.3	skate	13.3	skate	18.7	game clock	16.7
749	quill	book	21.3	paper	53.3	paper	22.7	paper	32.0
752	racket	fence	2.7	fence	8.0	bench	7.3	court	4.7
755	radio telescope	sky	6.0	sky	31.3	sky	20.0	sky	13.3
756	rain barrel	siding	4.7	siding	30.7	siding	12.7	siding	18.0
766	rotisserie	bread rolls	11.3	food baskets	19.3	window	14.7	bread rolls	18.0
767	eraser	marker	9.3	highlighter	16.7	sticky note	24.0	marker	6.0
771	safe	electronic devices	12.0	electronic devices	24.0	electronic devices	11.3	electronic devices	16.0
776	saxophone	bass guitar	4.0	music stand	4.0	photo	20.7	microphone	14.0
785	seat belt	driver	2.0	headrest	7.3	rearview mirror	6.0	driver	2.7
788	shoe store	mirror	10.0	poster	37.3	mirror	19.3	poster	22.0
792	shovel	soil	4.7	wheelbarrow	6.7	rock	8.0	garden tool	6.7
793	shower cap	comb	6.0	towel	19.3	mirror	6.7	comb	8.7
797	sleeping bag	tent	7.3	hiking boots	18.7	campsite	17.3	ground mat	14.7
801	snorkel	sand	9.3	beach	14.0	goggles	19.3	beach	23.3
802	snowmobile	trail markers	2.0	snow shovel	16.0	snow	68.0	snow shovel	8.0
803	snowplow	utility pole	2.0	road	8.0	snowdrift	21.3	snowdrift	6.0
822	steel drum	lamp	2.0	sunglass	10.0	guitar	5.3	guitar	8.0
827	stove	spoon	9.3	pan	20.0	sink	19.3	pan	16.7
867	semi-trailer truck	traffic light	4.0	pedestrian	12.7	pedestrian	6.0	concrete barrier	14.0
908	airplane wing	propeller	3.3	propeller	6.0	sea	2.0	sky	7.3
933	cheeseburger	burger wrapper	10.7	burger wrapper	25.3	burger wrapper	38.0	burger wrapper	36.0

Table 18: For each of the 100 selected Imagenet classes, we randomly sample 5000 images outside the class and apply SpurLens. We report the largest HR Gaps (as %, with $K = 50$) found and the associated spurious features.

Imagenet		Qwen2-VL		Llama 3.2		LLaVa 1.6		GPT-4o-mini	
Index	Name	Spur. Feat.	PA Gap	Spur. Feat.	PA Gap	Spur. Feat.	PA Gap	Spur. Feat.	PA Gap
0	tench	net	6.0	lure	2.7	lure	20.7	net	2.0
2	great white shark	swimmer	3.3	net	0.0	net	0.0	net	0.0
14	indigo bunting	feeder	7.3	branch	0.0	feeder	11.3	branch	0.0
42	agama	mud	0.7	tree	0.7	grass	31.3	stone	0.0
50	American alligator	water	1.3	tree	0.0	water	0.7	water	4.0
58	water snake	reed	4.0	reed	2.0	shell	3.3	shell	1.3
80	black grouse	grass	8.7	grass	2.7	tree	18.0	grass	3.3
81	ptarmigan	grass	24.0	snowdrift	6.0	grass	14.7	grass	9.3
82	ruffed grouse	moss	16.0	moss	3.3	moss	13.3	moss	8.7
89	sulphur-crested cockatoo	tree	2.0	feeder	0.0	tree	22.7	feeder	0.0
91	coucal	rock	1.3	grass	1.3	tree	30.7	grass	5.3
94	hummingbird	garden	0.7	sky	0.7	petal	32.7	tree	0.0
103	platypus	frog	2.0	sand	0.7	lily pads	1.3	lily pads	0.7
105	koala	branch	0.0	branch	0.0	foliage	6.0	foliage	2.0

Continued on the next page

Imagenet		Qwen2-VL		Llama 3.2		LLaVa 1.6		GPT-4o-mini	
Index	Name	Spur. Feat.	PA Gap	Spur. Feat.	PA Gap	Spur. Feat.	PA Gap	Spur. Feat.	PA Gap
147	grey whale	fisherman	14.7	surfboard	0.7	fisherman	4.0	surfboard	2.7
288	leopard	fence	0.0	fence	0.0	tree	6.0	fence	0.0
297	sloth bear	tree	14.0	tree	0.7	tree	45.3	waterhole	0.0
309	bee	leaf	2.0	flower	0.7	flower	5.3	leaf	2.0
313	stick insect	water droplet	6.0	dirt mound	0.0	dirt mound	0.0	dirt mound	0.0
324	small white butterfly	wildflower	11.3	tree	1.3	wildflower	14.7	leaf	2.0
325	sulphur butterfly	petal	22.0	petal	6.0	petal	36.7	garden	2.0
335	fox squirrel	acorn	2.7	acorn	0.7	tree	16.0	tree	0.0
351	hartebeest	muddy ground	0.0	tree	2.0	grass	6.7	muddy ground	0.0
364	three-toed sloth	tree	4.0	tree	0.7	tree	25.3	tree	0.0
379	howler monkey	tree	28.0	tree	0.7	tree	41.3	tree	4.0
384	indri	tree	2.0	rock	0.0	tree	41.3	tree	8.0
389	snoek fish	seaweed	24.0	sea surface	2.0	seaweed	30.0	rod	4.7
394	sturgeon	fish	32.0	fish	6.7	fish	48.7	fish	12.0
395	gar fish	turtle	26.0	turtle	11.3	turtle	50.0	bird	0.0
400	academic gown	diploma	27.3	diploma	30.7	diploma	32.0	diploma	25.3
415	bakery	car	2.7	car	5.3	car	3.3	car	1.3
416	balance beam	gymnast	73.3	gymnast	36.7	gymnast	44.7	rope	4.7
419	Band-Aid	blood	9.3	alcohol wipes	6.7	skin	6.7	ruler	4.0
424	barbershop	bus stop	4.0	bus stop	4.0	flowerpot	0.0	fire hydrant	0.7
425	barn	fence	2.0	birdhouse	11.3	fence	9.3	fence	2.7
433	swimming cap	towel	10.0	pool	2.0	snorkel	32.0	water bottle	2.7
434	bath towel	soap	30.0	soap	33.3	soap	38.7	soap	20.0
435	bathtub	shower cap	11.3	toilet	11.3	showerhead	2.7	shampoo	6.0
440	beer bottle	table	20.7	table	9.3	glass	14.0	cup	8.7
445	bikini	snorkel	28.0	pool	23.3	pool	24.0	snorkel	20.0
454	bookstore	clock	2.0	clock	6.7	picture frame	2.7	picture frame	1.3
465	bulletproof vest	gun	4.7	gun	2.0	helmet	22.7	floor	0.0
466	high-speed train	construction barriers	0.0	construction barriers	0.0	construction barriers	0.0	construction barriers	0.0
490	chain mail	sword stand	7.3	torch	4.7	sword stand	12.7	shield	2.0
491	chainsaw	work boots	4.7	woodpile	1.3	workbench	12.0	work boots	2.0
515	cowboy hat	horse	10.7	whip	7.3	guitar	16.7	whip	4.0
516	cradle	bedside table	5.3	stroller	10.0	infant toys	6.7	baby blanket	4.0
525	dam	waterfall	5.3	waterfall	6.7	waterfall	10.7	waterfall	5.3
537	dog sled	ski tracks	13.3	pine trees	0.7	pine trees	2.7	canoe	0.0
543	dumbbell	weight plate	2.7	weight plate	2.0	weight plate	3.3	weight plate	2.0
554	fireboat	paddle	2.0	pier	0.7	ramp	2.0	paddle	0.7
557	flagpole	building	12.7	building	20.0	building	13.3	building	10.7
563	fountain pen	paperclip	16.7	paper	16.0	paper	34.7	paper	8.7
565	freight car	road	6.0	road	8.7	road	22.0	grass	0.0
576	gondola	bridge	8.0	bridge	3.3	poster	12.7	tree	0.0
585	hair spray	shampoo	31.3	shampoo	17.3	shampoo	42.0	shampoo	5.3
588	hamper	wall	1.3	curtain	15.3	wall	12.0	curtain	6.0
592	hard disk drive	router	6.7	printer	12.7	router	7.3	desk	2.0
602	gymnastic horizontal bar	bench	15.3	bench	10.7	bench	13.3	banner	7.3
626	lighter	matchbox	26.0	cigarette	18.0	cigarette	25.3	keychain	1.3
655	miniskirt	tights	12.0	earring	6.0	tights	10.0	tights	10.7
667	graduation cap	diploma	31.3	diploma	30.0	diploma	36.0	diploma	30.0
671	mountain bike	water bottle	2.7	backpack	4.7	backpack	4.0	glove	2.0
678	neck brace	cup	2.7	remote	3.3	cup	2.0	wall	0.7
680	baby pacifier	teddy bear	16.0	diaper	4.0	crib	22.0	crib	2.0
682	obelisk	lamp post	11.3	statue	12.0	statue	20.0	pathway	2.0
684	ocarina	photo	1.3	microphone	2.7	headphone	2.7	headphone	0.0
695	padlock	wall	4.0	door	14.7	chain	25.3	wall	4.0
702	parallel bars	leotard	40.7	exercise bands	24.0	exercise bands	30.7	exercise bands	24.0
709	pencil case	notebook	19.3	notebook	12.0	notebook	14.7	notebook	6.0
720	pill bottle	tissue	14.7	tissue	11.3	thermometer	9.3	coffee cup	0.0
722	ping-pong ball	referee	4.7	scoreboard	2.7	racket	14.7	scoreboard	2.0
728	plastic bag	tissue	26.0	tissue	24.0	trash can	25.3	trash can	10.0
731	plunger	cleaner	11.3	brush	12.0	pipe	27.3	brush	1.3
733	pole	street	54.0	building	52.0	car	46.7	street	52.0
737	soda bottle	table	14.0	chair	18.0	cup	14.0	cup	13.3
738	plant pot	watering can	18.7	window	20.7	watering can	34.7	watering can	23.3
739	potter's wheel	sculpture	2.7	shelf	2.0	jug	6.7	jug	0.0
746	hockey puck	jersey	2.0	penalty box	2.7	skate	2.0	penalty box	1.3
749	quill	notebook	0.7	candle	2.0	notebook	15.3	ink bottle	4.7
752	racket	ball	21.3	ball	20.7	ball	22.0	ball	21.3
755	radio telescope	satellite	2.0	satellite	15.3	power lines	6.0	bench	0.0
756	rain barrel	potted plants	8.0	shed roof	13.3	garden statue	19.3	potted plants	4.7
766	rotisserie	cutlery	4.7	serving trays	4.7	cutlery	5.3	plant	0.0
767	eraser	notebook	14.7	notebook	12.7	paper	46.0	notebook	9.3
771	safe	electronic devices	1.3	bookshelf	14.7	clock	0.0	window	0.0
776	saxophone	guitar	6.0	guitar	2.7	guitar	4.7	amplifier	0.0
785	seat belt	headrest	15.3	rearview mirror	8.0	driver	8.7	dashboard	0.0
788	shoe store	vendor cart	7.3	clock	3.3	poster	2.0	vendor cart	2.7
792	shovel	wheel	16.0	wheel	11.3	wheel	23.3	wheel	14.0
793	shower cap	bathrobe	15.3	mirror	10.7	towel	62.7	towel	3.3
797	sleeping bag	camp chair	14.7	camp chair	11.3	camp chair	16.0	backpack	4.7

Continued on the next page

Imagenet		Qwen2-VL		Llama 3.2		LLaVa 1.6		GPT-4o-mini	
Index	Name	Spur. Feat.	PA Gap	Spur. Feat.	PA Gap	Spur. Feat.	PA Gap	Spur. Feat.	PA Gap
801	snorkel	buoy	8.7	buoy	12.7	wetsuit	13.3	beach	0.7
802	snowmobile	winter jacket	4.7	trail markers	4.7	trail markers	7.3	winter jacket	1.3
803	snowplow	shovel	8.7	glove	0.7	shovel	8.7	shovel	3.3
822	steel drum	speaker	10.7	fence	10.7	fence	11.3	beachball	0.7
827	stove	pan	18.0	dishwasher	17.3	pan	14.7	cabinet	12.7
867	semi-trailer truck	construction site	16.7	construction site	22.0	construction site	40.7	construction site	5.3
908	airplane wing	propeller	5.3	propeller	4.7	propeller	3.3	propeller	1.3
933	cheeseburger	napkin	0.0	burger wrapper	2.0	burger wrapper	2.0	napkin	0.0